

# Persistent currents in Bose-Bose mixtures after an interspecies interaction quench

D. Spehner<sup>1,2</sup>, L. Morales-Molina<sup>3</sup>, and S. A. Reyes<sup>3</sup>

<sup>1</sup>Departamento de Ingeniería Matemática, Universidad de Concepción, Concepción, Chile

<sup>2</sup>Univ. Grenoble Alpes, CNRS, Institut Fourier and LPMMC, F-38000 Grenoble, France

<sup>3</sup>Facultad de Física, Pontificia Universidad Católica de Chile, Casilla 306, Santiago, Chile

February 5, 2022

## Abstract

We study the persistent currents and interspecies entanglement generation in a Bose-Bose mixture formed by two atomic gases (hereafter labelled by the letters  $A$  and  $B$ ) trapped in a one-dimensional ring lattice potential with an artificial gauge field after a sudden quench from zero to strong interactions between the two gases. Assuming that the strength of these interactions is much larger than the single species energies and that the gas  $A$  is initially in the Mott-insulator regime, we show that the current of the gas  $B$  is reduced with respect to its value prior the interaction quench. Averaging fast oscillations out, the relative decrease of this current is independent of the initial visibility and Peierls phase of the gas  $B$  and behaves quadratically with the visibility of the gas  $A$ . The second Rényi entropy of the reduced state measuring the amount of entanglement between the two gases is found to scale linearly with the number of sites and to be proportional to the relative decrease of the current.

## 1 Introduction.

The manifestations of quantum coherence and entanglement in many-body systems is one of the most challenging problems in condensed matter physics and quantum technology. The recent experimental realizations with trapped ultracold atoms of analogs of electronic mesoscopic systems such as superconducting quantum interference devices [1, 2, 3] has opened new perspectives in the study of matter-wave interferences. Atomtronics focuses on the design of such atomic quantum devices, characterized by tunable parameters and low decoherence, and their applications to fundamental research and technology [4, 5].

One of the striking manifestation of quantum interferences is the Aharonov-Bohm effect. In a ring pierced by a magnetic flux, this gives rise to persistent currents varying periodically with the flux, which were observed long ago in superconductors and normal metals [6, 7, 8, 9]. In atomic Bose-Einstein condensates (BECs) trapped in a ring-shaped potential, an artificial gauge field can be induced by laser fields or by the Coriolis force in the presence of a rotating potential barrier [10]. This system provides a novel platform for studying persistent currents [11, 12, 13, 14]. It encompasses a rich variety of quantum phenomena, including the formation of macroscopic superpositions of clockwise and anticlockwise flowing states at specific values of the magnetic flux when rotation invariance is broken by a localized potential barrier [15, 16, 17, 18, 19]. The influence of such a barrier on the current amplitude has been studied in Refs. [13, 14] for all strengths of the repulsive atomic interactions and in Ref. [20] for attractive interactions. The time evolutions of the persistent current and of space correlations when the gas is either slowly driven across the Superfluid (SF) to Mott-Insulator (MI) transition or is subject to an interaction quench crossing this transition have been also investigated [21, 22].

The quantum interference effects become more complex when two atomic species are involved. It is known that mixtures of two condensates can lead to the generation of exotic phases and to the formation of quantum droplets, among others phenomena [23, 24, 25, 26, 27, 28, 29, 30, 31]. It has been conjectured that the phase coherences of the two atomic gases in the mixing process may play a crucial role in these emerging phenomena [26, 27]. A number of theoretical and experimental works have focused on quantum phases in optical lattices, in particular because of the analogy with condensed matter systems [32, 33, 34, 35, 36, 37, 38, 39, 40]. For repulsive interspecies interactions, phase separation processes have been investigated thoroughly (see e.g. [41, 42] and references therein for spectral and density profile analyses and [43] for quench dynamics crossing the miscibility to immiscibility transition). More recently, Bose-Bose mixtures consisting of a single atom interacting with a gas of atoms of a different species have attracted a lot of attention due to the formation of polarons in such systems [44, 45, 46, 47, 48].

A particular emphasis in the study of multi-component quantum gases concerns out-of-equilibrium dynamics following a sudden quench. Such quench dynamics can be investigated experimentally thanks to the high level of control on the trapping potential and the ability to tune (and even change the sign of) the intra- and inter-species interactions using Feshbach resonances [49, 50, 51]. On the theoretical side, special attention has been devoted to interaction quenches (inter-species interactions are suddenly switched on) [52, 53, 43, 47]. In these works, the generation of entanglement in the quench dynamics and its role in the observed phenomena have been investigated.

In the different context of the quench dynamics of a single component gas trapped in an infinite 1D-lattice, it has been shown that the entanglement associated to a partition of the lattice into a finite block of size  $\ell$  and its complement, quantified by the von Neumann entropy of the reduced state, saturates to a value proportional to  $\ell$  after a linear growth with time [54]. Such a behavior of the entanglement after the quench has been observed experimentally for small lattice sizes in measurements of the 2-Rényi entropy of entanglement [55].

Coming back to persistent currents in BECs, it is natural to ask about the effect on the current of the first atomic species of the presence of a second atomic gas trapped in the same ring. In order to change this current, the two quantum gases must interact and be entangled with each other. One may then wonder whether the variation of the current provides in some way a measure of the amount of entanglement between the two gases. Another natural question concerns the dependence of the persistent current on the phase coherence of the two gases before they start to interact.

In this article, we investigate these questions by considering a binary mixture containing two bosonic atomic species  $A$  and  $B$  (which may either correspond to different types of atoms or to identical atoms in different internal states) trapped in a 1D-ring lattice potential in the presence of an artificial gauge field. Assuming that the two species are initially decoupled and that the gas  $A$  is in the MI regime, we calculate analytically and numerically the time evolution of the current of  $B$ -atoms and the generation of entanglement between the  $A$  and  $B$ -condensates after a sudden quench from zero to strong inter-species interactions. We quantify the amount of entanglement using the Schmidt number [56] shifted by one,  $\mathcal{K}_{AB} = \text{tr}_A[(\text{tr}_B |\psi_{AB}\rangle\langle\psi_{AB}|)^2]^{-1} - 1$ , where  $|\psi_{AB}\rangle$  is the wavefunction of the binary mixture after the interaction quench. For small  $\mathcal{K}_{AB}$  this quantity is nearly equal to the 2-Rényi entropy of entanglement  $S_{AB}^{(2)} = \ln(1 + \mathcal{K}_{AB})$  [57], which is a measure of entanglement having similar properties as the entanglement of formation (von Neumann entropy of the reduced state). It has been shown recently that  $S_{AB}^{(2)}$  can be determined from statistical correlations between random measurements [58, 59, 60] (see also [61] for a measurement protocol of the 2-Rényi entropy, which can be applied in our setup to determine  $S_{AB}^{(2)}$  in view of the possibility to monitor different trapping potentials for each species).

Our main results can be described as follows. We show that the  $B$ -current after the quench is reduced due to interactions with the gas  $A$ . Averaging out the fast oscillations with frequency equal to the inter-species interaction energy divided by the Planck constant, we prove that the relative variation  $\langle \mathcal{J}_B \rangle$  of the  $B$ -current before and after the quench and the shifted Schmidt number  $\langle \mathcal{K}_{AB} \rangle$  are proportional to each

other and follow some universal laws. In particular,  $\langle \mathcal{J}_B \rangle$  is independent of the visibility of the gas  $B$  before the quench, being the same when the latter is in the MI or in the SF regimes, and does also not depend on the Peierls phase of the  $B$ -atoms. On the other hand,  $\langle \mathcal{J}_B \rangle$  behaves quadratically with the initial visibility of the gas  $A$ . Furthermore,  $\langle \mathcal{K}_{AB} \rangle$  and  $S_{AB}^{(2)}$  are linear in the number of lattice sites  $L$  and  $\langle \mathcal{K}_{AB} \rangle / L = \beta \langle \mathcal{J}_B \rangle$ , with a proportionality factor  $\beta$  depending only on the filling factor  $\nu_B$ , the Peierls phase, and the initial visibility of the gas  $B$  when this gas is in the MI regime, whereas when it is in the SF regime  $\beta$  depends on the filling factor  $\nu_B$  only. We show that the generation of entanglement in the quench dynamics and its universal relation with the reduction of the  $B$ -current comes from particle-hole excitations in the gas  $A$  which slow down the flow of  $B$ -atoms and are coupled to site-dependent wavefunctions of the gas  $B$ . We argue that these results could be used for determining the amount of entanglement between the two gases from quantities (atomic current and visibility of interference fringes) that can be measured experimentally (see e.g. [62, 63, 64, 12] for the observation of the supercurrent of a single-component gas in ring-shape trapping potentials).

Let us comment on the methods used to obtain the aforementioned results. Our analytical calculations rely on (i) a perturbative expansion of the initial ground state and (ii) small and intermediate time approximations for the time propagator, valid when the inter-species interaction strength is much larger than the tunneling and intra-species interaction energies. We point out that the method employed to determine the Schmidt number in Sec. 7 is original and could be useful in other contexts. It consists in expressing  $\mathcal{K}_{AB}(t)$  when the gas  $A$  is in the MI regime in terms of an effective propagator acting on the other gas (see Appendix B); by diagonalizing perturbatively the Hamiltonian in this propagator for large inter-species interactions, we are able to determine  $\mathcal{K}_{AB}(t)$  at times of the order of the inverse tunneling and intra-species interaction energies of the gas  $B$ . Our numerical simulations, in turn, rely on exact diagonalization. Although they are carried out for small lattice sizes, these simulations corroborate the analytical results which apply to much larger atom numbers and lattice sizes. This implies that finite size effects are not relevant for the physical effects we are interested in, thus enabling their applications to mesoscopic systems of arbitrary size.

The paper is organized as follows. We introduce our model of a Bose-Bose mixture in a 1D-ring lattice in Sect. 2. Section 3 is devoted to a brief discussion on the visibility of a single species before the interaction quench and its behavior as function of the Peierls phase for finite lattice sizes. The calculation of the  $B$ -current after the interaction quench is performed in Sec. 4. We determine in Sec. 5 the entanglement generation between the two gases and show there that the time-averaged shifted Schmidt number  $\langle \mathcal{K}_{AB} \rangle$  is proportional to  $L$  and to  $\langle \mathcal{J}_B \rangle$ , assuming an averaging time much larger than the inverse inter-species interaction energy and much smaller than the inverse single species energies. In Sec. 6 we show that quantum superpositions in the post-quench total wavefunction involving particle-hole excitations in the gas  $A$  are at the origin of the entanglement. In Sec. 7, we evaluate the Schmidt number at larger times and show that its average  $\langle \mathcal{K}_{AB} \rangle_t$  remains constants over a large time period, suggesting a convergence of  $\langle \mathcal{K}_{AB} \rangle_t$  at large times  $t$  to universal values which are determined analytically. Concluding remarks are given in Sec. 8. Some technical details on the analytical calculations are presented in the two appendices.

## 2 Model

Let us consider two atomic gases  $A$  and  $B$  trapped in the same 1D-ring lattice potential with  $L$  sites. We denote by  $\hat{a}_j^\dagger$ ,  $\hat{a}_j$ , and  $\hat{n}_j^A = \hat{a}_j^\dagger \hat{a}_j$  the creation, annihilation, and number operators at site  $j$  for atoms of the gas  $A$ , and by  $\hat{b}_j^\dagger$ ,  $\hat{b}_j$ , and  $\hat{n}_j^B$  the corresponding operators for the gas  $B$ . The two gases are described by Bose-Hubbard Hamiltonians, e.g. for the gas  $A$

$$\hat{H}_A = -J_A \sum_j (e^{i\phi_A} \hat{a}_{j+1}^\dagger \hat{a}_j + \text{h.c.}) + \frac{U_A}{2} \sum_j \hat{n}_j^A (\hat{n}_j^A - 1) = \hat{K}_A + \hat{H}_A^{\text{int}}, \quad (1)$$

where  $J_A$  and  $U_A$  are the tunneling and interaction energy strengths and  $\phi_A$  is the Peierls phase associated to an artificial gauge field. The sums in (1) run over all lattice sites  $j = 0, \dots, L - 1$  and “h.c.” refers to the Hermitian conjugate operator. To account for the periodic boundary condition the sites  $L$  and  $0$  are identified with each other. The Hamiltonian  $\hat{H}_B$  of the gas  $B$  is given similarly in terms of  $J_B$ ,  $U_B$ , and  $\phi_B$ . We consider repulsive intra-species interactions,  $U_A, U_B > 0$ , and assume fixed total atom numbers  $N_A, N_B$  for each species with integer filling factors  $\nu_A = N_A/L$ ,  $\nu_B = N_B/L$ . The two gases are initially uncorrelated and in their ground states (GSs)  $|\psi_A\rangle$  and  $|\psi_B\rangle$ . At time  $t = 0$ , attractive interactions between the two species are suddenly switched on (see the left panel in Fig. 1). The mixture subsequently evolves according to the Hamiltonian ( $V > 0$ )

$$\hat{H}_{AB} = \hat{H}_A \otimes \hat{\mathbf{1}}_B + \hat{\mathbf{1}}_A \otimes \hat{H}_B + \hat{H}_{AB}^{\text{int}} \quad , \quad \hat{H}_{AB}^{\text{int}} = -V \sum_j \hat{n}_j^A \hat{n}_j^B . \quad (2)$$

We assume that inter-species interactions are much larger than the single species energies and that the gas  $A$  is initially in the MI regime, i.e.,

$$V \gg U_A, U_B, J_B \quad , \quad \lambda_A = \frac{J_A}{U_A} \ll 1 . \quad (3)$$

The gas  $B$  can be either in the MI or the SF regime; in fact both cases  $\lambda_B \ll 1$  and  $\lambda_B \gtrsim 1$  will be analyzed in what follows.

We will study in this work the time evolutions of the persistent current of  $B$ -atoms (called in what follows the  $B$ -current) and of the amount of  $A$ - $B$  entanglement after the interaction quench. The  $B$ -current is given at time  $t \geq 0$  by  $I_B(t) = \text{tr}_B[\hat{\rho}_B(t)\hat{I}_B]$  with  $\hat{\rho}_B(t) = \text{tr}_A|\psi_{AB}(t)\rangle\langle\psi_{AB}(t)|$  the reduced density matrix of the gas  $B$ ,  $|\psi_{AB}(t)\rangle$  the time-evolved state of the mixture with the Hamiltonian (2), and  $\hat{I}_B$  the current operator

$$\hat{I}_B = \frac{1}{2LJ_B} \frac{\partial \hat{H}_B}{\partial \phi_B} = \frac{1}{2iL} \sum_j (\hat{b}_{j+1}^\dagger \hat{b}_j e^{i\phi_B} - \text{h.c.}) \quad (4)$$

(here  $\hbar = 1$ ). We will focus in the following on the relative variation of  $B$ -current and its average in the time interval  $[0, t]$ , defined by

$$\mathcal{J}_B(t) = \frac{I_B(0) - I_B(t)}{I_B(0)} \quad , \quad \langle \mathcal{J}_B \rangle_t = \frac{1}{t} \int_0^t dt' \mathcal{J}_B(t') . \quad (5)$$

When the tunnelling energy of the gas  $A$  vanishes (i.e. when  $J_A = 0$ ), the  $B$ -current is time-independent and thus  $\mathcal{J}_B(t) = 0$ . Actually, then the initial state  $|\psi_A\rangle|\psi_B\rangle$  of the mixture has  $\nu_A$  atoms  $A$  per site and the coupling  $\hat{H}_{AB}^{\text{int}}$  acts on it as  $-V\nu_A N_B$ , where the total number  $N_B = \sum_j \hat{n}_j^B$  of  $B$ -atoms is a  $c$ -number; hence  $|\psi_{AB}(t)\rangle$  is equal to  $|\psi_A\rangle|\psi_B\rangle$  at all times  $t$  up to irrelevant phases. In contrast, when  $J_A > 0$  the initial GS of the gas  $A$  has particle-hole excitations [65], thus the coupling entangles the two gases and the  $B$ -current is modified,  $\mathcal{J}_B(t) \neq 0$ .

The time evolution of the relative  $B$ -current variation, obtained numerically from exact diagonalizations of  $\hat{H}_A$ ,  $\hat{H}_B$ , and  $\hat{H}_{AB}$ , is shown in the right panel of Fig. 1. We use a second-order Suzuki-Trotter decomposition method with time steps as small as  $\Delta t = 0.002$ . We observe that  $\mathcal{J}_B(t)$  presents fast oscillations of period  $2\pi/V$  superimposed on a complex pattern with oscillations with larger periods [66]. The time-averaged version of  $\mathcal{J}_B(t)$  displays two plateaus: the first one at times  $V^{-1} \ll t \ll U_A^{-1}, U_B^{-1}, J_B^{-1}$ , the second one at times of the order of the single species inverse energies. We will show analytically in Sec. 4 that the value of the first plateau does not depend on the initial state of the gas  $B$ . Note that this universal value holds for the relative variation of the  $B$ -current defined in (5); in contrast, the  $B$ -current strongly depends on the initial state of the gas  $B$ , being much smaller when  $B$  is in the MI regime than when it is in the SF regime.

Before calculating the  $B$ -current, we study the visibility of a single atomic species in a ring lattice with a gauge field before the interaction quench.

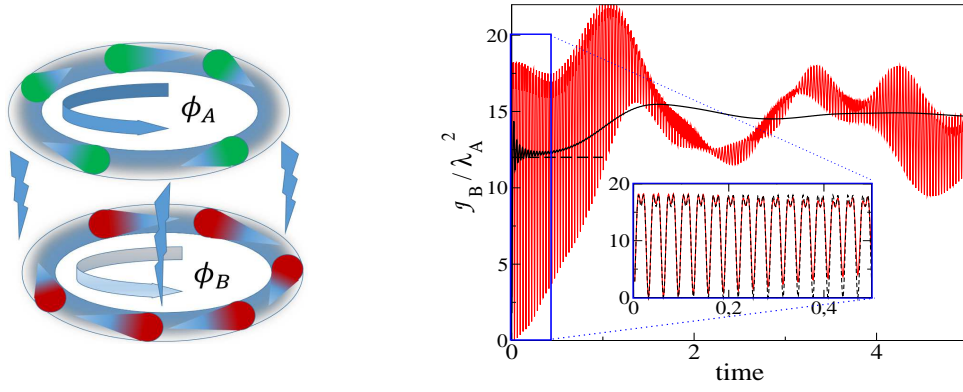


Figure 1: **Left panel:** Sketch of moving atoms on a 1D-ring lattice with two interacting species  $A$  and  $B$  represented by green and red balls, in the presence of Peierls phases  $\phi_A$  and  $\phi_B$ . **Right panel:** Time evolution after the interaction quench of the relative  $B$ -current variation  $\mathcal{J}_B(t)$  (red curve) and its time-average (black curve), Eq. (5), divided by  $\lambda_A^2$  for a lattice with  $L = 4$  sites,  $N_A = N_B = 4$  atoms of each species,  $V = 200U_B$ ,  $J_B = U_A = U_B$ ,  $J_A = 0.05U_B$ ,  $\phi_A = \phi_B = \pi/10$  (from numerical calculations). Time is in units of  $U_B^{-1}$ . Dashed horizontal segment: universal value of Eq. (19). **Inset:** amplification of the blue box shown in the figure with formula (18) displayed in dashed line.

### 3 Single species visibility

A good indicator of the degree of phase coherence of a single species (say  $B$ ) is the visibility. The latter is estimated experimentally by measuring the interference pattern after a free expansion of the gas. It is defined as  $\mathcal{V}_B = (S_{\max} - S_{\min}) / (S_{\max} + S_{\min})$ ,  $S_{\max}$  and  $S_{\min}$  being the maximum and minimum of the momentum distribution  $S(q) = \sum_{i,j} e^{iq(i-j)} \langle \psi_B | \hat{b}_i^\dagger \hat{b}_j | \psi_B \rangle$ . For  $J_B = 0$ , the GS of the gas  $B$  is the phase-incoherent MI state  $|\psi_B\rangle = |\psi_{\text{MI}}\rangle$  having  $\nu_B$  atoms per site [65]. Then  $\mathcal{V}_B = 0$  (no interference fringes) and the  $B$ -current  $\langle \psi_B | \hat{I}_B | \psi_B \rangle$  vanishes. Increasing the energy ratio  $\lambda_B = J_B / U_B$ , the visibility and current increase, with  $\mathcal{V}_B$  reaching its maximum  $\mathcal{V}_B = 1$  in the SF limit  $\lambda_B \gg 1$ .

It has been shown both theoretically and experimentally [65, 67] that the visibility of a single BEC trapped in an infinite gauge-free lattice potential behaves linearly with  $\lambda_B$  when  $\lambda_B \lesssim 1$ . However, we will need in the sequel the visibility for finite lattice sizes in the presence of a gauge field and cannot rely on the results of these references. In the MI regime  $\lambda_B \ll 1$ , one obtains by expanding perturbatively the GS  $|\psi_B\rangle$  and the momentum distribution up to second order in  $\lambda_B$  that (see Appendix A)

$$\mathcal{V}_B = 4(\nu_B + 1)\lambda_B v_L(\phi_B) [1 - (4\nu_B + 1)\lambda_B w_L(\phi_B)] + \mathcal{O}(\lambda_B^3) \quad (6)$$

with

$$v_L(\phi_B) = \begin{cases} \cos(\phi_B - \ell\phi_0) & \text{if } L \text{ is even} \\ \frac{1}{2}(\cos(\phi_B - \ell\phi_0) + \cos(\frac{1+2k}{2}\phi_0 - \phi_B)) & \text{if } L \text{ is odd} \end{cases} \quad (7)$$

$$w_L(\phi_B) = \begin{cases} 0 & \text{if } L \text{ is even} \\ -\cos(\phi_B - \ell\phi_0) + \cos(\frac{1+2k}{2}\phi_0 - \phi_B) & \text{if } L \text{ is odd,} \end{cases} \quad (8)$$

where  $\phi_0 = 2\pi/L$  is the lattice flux,  $\ell = E[\phi_B/\phi_0 + 1/2]$  the angular momentum of the SF state, and  $k = E[\phi_B/\phi_0]$  (here  $E$  is the integer part). Note that Gauge invariance implies that  $\mathcal{V}_B$  is periodic in the Peierls phase  $\phi_B$  with period  $\phi_0$ . In the limit  $L \rightarrow \infty$  one finds that  $v_L(\phi_B), w_L(\phi_B) \rightarrow 1$  for any  $\phi_B$ , so that  $\mathcal{V}_B$  becomes phase independent and one recovers the result of Refs. [65, 67]. It is easy to show

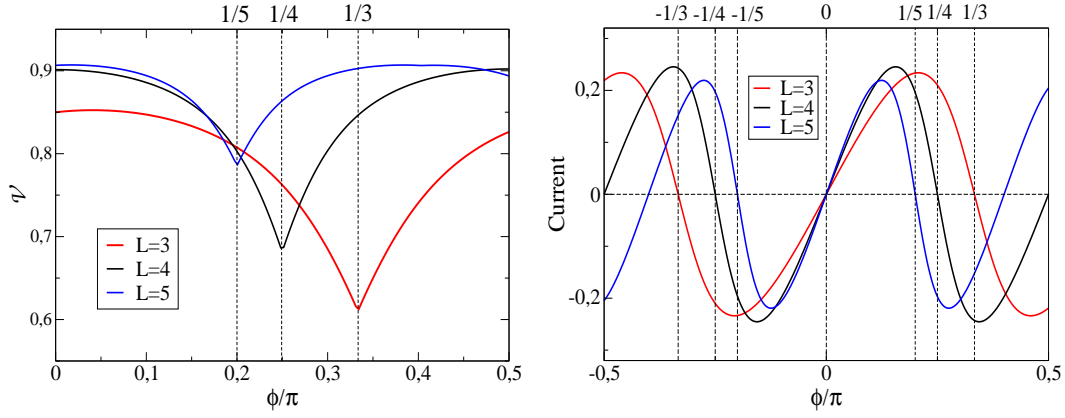


Figure 2: **Left panel:** Visibility of a Bose gas with a single species  $B$  trapped in a 1D-ring lattice potential as function of the Peierls phase  $\phi_B$  for  $\lambda_B = J_B/U_B = 0.2$  and  $N_B = L = 3, 4$ , and  $5$  (from numerical calculations). **Right panel:**  $B$ -current  $I_B(0)$  (in arbitrary units) of the gas  $B$  prior the interaction quench as function of  $\phi_B$  for the same parameters. The value of  $\lambda_B$  is close to the transition between the MI and SF regimes.

from (6)-(8) that for finite lattice sizes  $L$ , the visibility  $\mathcal{V}_B$  reaches its minimum when  $\phi_B$  is equal to a half-integer value of  $\phi_0$  (see Appendix A).

In the opposite limit of weak interactions  $U_B \ll J_B$  (SF regime  $\lambda_B \gg 1$ ), when  $\phi_B$  is not close to a half-integer value of  $\phi_0$  the GS of the Bose-Hubbard Hamiltonian can be approximated by the SF state (GS of the tunneling Hamiltonian). Since the visibility in the latter state is equal to 1 for all  $\phi_B$ 's, it follows that  $\mathcal{V}_B = 1 + \mathcal{O}(\lambda_B^{-1})$ . The phases  $\phi_B = (\ell + 1/2)\phi_0$ ,  $\ell = 0, \pm 1, \dots$ , are the points where the parabola giving the energies of the SF states with angular momenta  $\ell$  and  $\ell + 1$  intersect. For such phases, quantum fluctuations of angular momentum produce fluctuations in the speed of rotation of the gas which are expected to blur the interference pattern, henceforth reducing the visibility as compared to its value when  $\phi_B$  is not close to a half-integer value of  $\phi_0$ . This is confirmed by numerical simulations for  $L = 3, 4$ , and  $5$  (not shown here).

Comparing with our aforementioned result in the MI regime, we conjecture that  $\mathcal{V}_B$  is minimum at Peierls phases equal to half-integer values of  $\phi_0$  for any energy ratio  $\lambda_B$ . This is supported by numerical calculations. For instance, one observes in the left panel of Fig. 2 that  $\mathcal{V}_B$  presents a well pronounced minimum at  $\phi_B = \phi_0/2 = \pi/L$  when  $L = 3, 4$ , and  $5$  for  $\lambda_B = 0.2$ . Note that the phase points  $(\ell + 1/2)\phi_0$  are singled out by the behavior of the GS persistent current  $I_B(0) = \langle \psi_B | \hat{I}_B | \psi_B \rangle$  of the Bose gas as function of  $\phi_B$ . The latter is periodic with period  $\phi_0$  and drops rapidly and changes sign at these phase points, independently of the strength of the repulsive interactions (i.e., of  $\lambda_B$ ) [15, 20]. For reference, the behavior of  $I_B(0)$  as function of  $\phi_B$  is shown in the right panel in Fig. 2.

Note that in Fig. 2 the depth of the minima of  $\mathcal{V}_B$  become less pronounced as  $L$  is increased, in agreement with the expectation that the visibility is phase independent for an infinite ring. Let us stress that the numerical simulations carried out in this work consider small lattice sizes. This enables us to observe the dependence of physical quantities like the visibility on the Peierls phase, whose effect vanishes at large sizes.

## 4 The $B$ -current

We can calculate the  $B$ -current at times  $t \ll U_A^{-1}, U_B^{-1}, J_B^{-1}$  as follows. Using the invariance of the reduced density matrix  $\hat{\rho}_B(t)$  with respect to translations by one lattice site and introducing the eigenstates

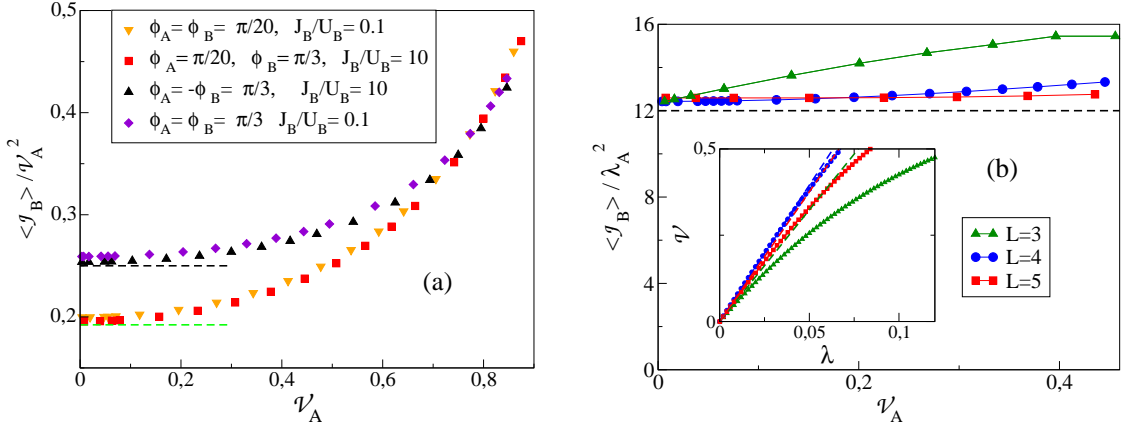


Figure 3: **(a)** Time averaged current variation  $\langle \mathcal{J}_B \rangle_t$  divided by the square visibility  $\mathcal{V}_A^2$  vs.  $\mathcal{V}_A$  for different values of  $\lambda_B = J_B/U_B$  and Peierls phases, from numerical calculations with  $L = N_A = N_B = 4$ . The average is up to time  $t = 0.3/U_B$ . Triangles downward:  $V = 100U_B$ ,  $U_A = U_B$ ,  $J_B = 0.1U_B$ ,  $\phi_A = \phi_B = \pi/20$ . Squares:  $V = 1000U_B$ ,  $U_A = J_B = 10U_B$ ,  $\phi_A = \pi/20$ ,  $\phi_B = \pi/3$ . Triangles upward:  $V = 1000U_B$ ,  $U_A = J_B = 10U_B$ ,  $\phi_A = -\phi_B = \pi/3$ . Diamonds:  $V = 100U_B$ ,  $U_A = U_B$ ,  $J_B = 0.1U_B$ ,  $\phi_A = \phi_B = \pi/3$ . In all cases  $J_A$  is varied in order to change  $\mathcal{V}_A^2$ . The horizontal segments correspond to the values in the RHS of Eq.(19). **(b)**  $\langle \mathcal{J}_B \rangle_t$  divided by  $\lambda_A^2$  for  $V = 100U_B$ ,  $U_A = U_B$ ,  $J_B = 0.1U_B$ ,  $J_A$  variable,  $\phi_A = \phi_B = \pi/20$ , and different site numbers  $L = N_A = N_B = 3, 4$  and 5. The horizontal dashed line corresponds to the first equality in Eq.(19). **Inset:** single species visibility vs  $\lambda = J/U$  for the same values of  $L$  and  $N$ , with dashed lines showing the linear term in Eq. (6).

$|\underline{n}_B\rangle = |n_0^B, \dots, n_{L-1}^B\rangle$  of  $\hat{n}_B = (\hat{n}_0^B, \dots, \hat{n}_{L-1}^B)$  (Fock states), one has

$$I_B(t) = \text{Im} \sum_{\underline{n}_B} \sqrt{n_0^B(n_1^B + 1)} e^{i\phi_B} \langle \underline{n}_B | \hat{\rho}_B(t) | \underline{n}_B + \mathbf{1}_1 - \mathbf{1}_0 \rangle, \quad (9)$$

where  $\mathbf{1}_i$  denotes the vector with components  $\delta_{ij}$ ,  $j = 0, \dots, L-1$ , and the sum runs over all  $\underline{n}_B \in \mathbb{N}^L$ ,  $\sum_j n_j^B = N_B$ . Due to our small time hypothesis, hopping and intra-species interactions can be neglected in the Hamiltonian (2) and the dynamics is solely governed by inter-species interactions. Thus  $|\psi_{AB}(t)\rangle = e^{itV\hat{n}_A \cdot \hat{n}_B} |\psi_A\rangle |\psi_B\rangle$ . Plugging this expression into (9), the current can be cast as

$$I_B(t) = I_B(0) \langle e^{-itV\Delta\hat{n}_{01}^A} \rangle_{\psi_A}, \quad \Delta\hat{n}_{01}^A = \hat{n}_1^A - \hat{n}_0^A, \quad (10)$$

where  $I_B(0)$  is the current in the GS of  $\hat{H}_B$  (obtained by substituting  $\hat{\rho}_B(t)$  by  $|\psi_B\rangle\langle\psi_B|$  in (9)),  $\langle \cdot \rangle_{\psi_A} = \langle \psi_A | \cdot | \psi_A \rangle$  is the quantum expectation in  $|\psi_A\rangle$ , and we have used that  $\langle e^{-itV\Delta\hat{n}_{01}^A} \rangle_{\psi_A}$  is real, as will be shown below. The relative current variation reads

$$\mathcal{J}_B(t) = 1 - \langle e^{-itV\Delta\hat{n}_{01}^A} \rangle_{\psi_A}, \quad t \ll U_A^{-1}, U_B^{-1}, J_B^{-1}. \quad (11)$$

It follows from the Cauchy-Schwarz inequality that  $\mathcal{J}_B(t) \geq 0$ . Hence the effect of the inter-species coupling at time  $t > 0$  is to reduce the currents of each species. Furthermore, the relative current variation  $\mathcal{J}_B(t)$  does not depend on the initial GS of the gas  $B$ , being the same when  $B$  is initially in the SF or MI regimes, and is also independent of the Peierls phase  $\phi_B$  of the gas  $B$ . This independence of the relative variation of  $B$ -current after the interaction quench from  $\phi_B$  and  $\lambda_B$  contrasts with the behavior of the  $B$ -current  $I_B(0)$  before the quench. The latter oscillates with  $\phi_B$  (see the right panel in Fig. 2) with

an amplitude which strongly depends on the visibility  $\mathcal{V}_B$ , i.e., on  $\lambda_B$  (see the discussion at the beginning of Sec. 3). The independence of  $\mathcal{J}_B(t)$  from  $\lambda_B$  and  $\phi_B$  is confirmed by the numerical results displayed in Fig. 3(a). Indeed, one sees in this figure that the time-averaged values  $\langle \mathcal{J}_B \rangle_t$  of  $\mathcal{J}_B(t)$  for  $\lambda_B = 10$ ,  $\phi_B = \pi/3$  and for  $\lambda_B = 0.1$ ,  $\phi_B = \pi/20$  are very close from each other, for all values of the visibility  $\mathcal{V}_A$  of the gas  $A$ . As we shall explain below, the observed dependence of  $\langle \mathcal{J}_B \rangle_t / \mathcal{V}_A$  on the Peierls phase  $\phi_A$  of the gas  $A$  for small  $\mathcal{V}_A$  originates from the variation of  $\mathcal{V}_A$  with  $\phi_A$  predicted by Eq. (6); this is thus a finite-size effect.

We next calculate the  $A$ -expectation in (11), assuming that the gas  $A$  is in the MI regime ( $\lambda_A \ll 1$ ), and show in the way that it is real up to second order in  $\lambda_A$ . (Let us note that although this is true for all values of  $\lambda_A$  when  $\phi_A = 0$  by symmetry of  $\hat{H}_A$  under  $j \mapsto L - j \pmod{L}$ , this is not the case for  $\phi_A \neq 0$  and large  $\lambda_A$ .) The GS of  $\hat{H}_A$  can be evaluated by treating the tunneling Hamiltonian  $\hat{K}_A$  in (1) perturbatively. The unperturbed Hamiltonian  $\hat{H}_A^{\text{int}}$  has eigenvectors  $|\underline{n}_A\rangle$ , eigenenergies  $E_A^{(0)}(\underline{n}_A)$ , and GS  $|\psi_{\text{MI}}\rangle = |\underline{n}_A\rangle$  with  $\underline{n}_A = (\nu_A, \dots, \nu_A)$ . Noting that the energy to create a particle-hole excitation is  $E_A^{(0)}(\underline{n}_A \pm 1_{i+1} \mp 1_i) - E_A^{(0)}(\underline{n}_A) = U_A$ , one finds

$$|\psi_A\rangle = |\psi_{\text{MI}}\rangle + \lambda_A |\psi_A^{(1)}\rangle + \lambda_A^2 |\psi_A^{(2)}\rangle + \mathcal{O}(\lambda_A^3), \quad (12)$$

where the first-order correction is

$$|\psi_A^{(1)}\rangle = -\frac{1}{J_A} \hat{K}_A |\psi_{\text{MI}}\rangle = \sum_j (e^{i\phi_A} \hat{a}_{j+1}^\dagger \hat{a}_j + \text{h.c.}) |\psi_{\text{MI}}\rangle \quad (13)$$

and the second-order correction satisfies (see appendix A)

$$\langle \psi_{\text{MI}} | \psi_A^{(2)} \rangle = -\alpha_A L \quad \text{with} \quad \alpha_A = \nu_A(\nu_A + 1). \quad (14)$$

A simple calculation yields

$$\langle e^{-itV\Delta\hat{n}_{01}^A} \rangle_{\psi_A^{(1)}} \equiv \langle \psi_A^{(1)} | e^{-itV\Delta\hat{n}_{01}^A} | \psi_A^{(1)} \rangle = 2\alpha_A \sum_j \cos(tV\Delta_{01}^{j,j+1}), \quad (15)$$

where  $\pm\Delta_{01}^{j,j+1}$  stands for the eigenvalue of  $\Delta\hat{n}_{01}^A$  in the particle-hole excitation state

$$|\varphi_{A,j,\pm}\rangle = |\underline{n}_A \pm 1_{j+1} \mp 1_j\rangle. \quad (16)$$

Since  $\Delta_{01}^{j,j+1} = \delta_{j+1,1} - \delta_{j,1} - \delta_{j+1,0} + \delta_{j,0}$  equals 2 if  $j = 0$ ,  $\Delta_{01}^{j,j+1} = -1$  if  $j = 1$  or  $L - 1$ , and  $\Delta_{01}^{j,j+1} = 0$  otherwise, one finds

$$\langle e^{-itV\Delta\hat{n}_{01}^A} \rangle_{\psi_A^{(1)}} = 2\alpha_A [L - 3 + 2\cos(tV) + \cos(2tV)]. \quad (17)$$

Using (11), (14), (17),  $e^{-itV\Delta\hat{n}_{01}^A} |\psi_{\text{MI}}\rangle = |\psi_{\text{MI}}\rangle$ , and  $\langle \psi_A^{(1)} | \psi_{\text{MI}} \rangle = 0$ , this gives

$$\mathcal{J}_B(t) = 2\alpha_A \lambda_A^2 [3 - 2\cos(tV) - \cos(2tV)] + \mathcal{O}(\lambda_A^3). \quad (18)$$

A good agreement between Eq. (18) and the numerical result at times  $t \ll 1/U_A, 1/U_B, 1/J_B$  is seen in Fig. 1 (inset, right panel). The cosines disappear upon averaging up to a time  $t$  much larger than  $1/V$ , with  $t \ll 1/U_A, 1/U_B, 1/J_B$ . Plugging the expression of the visibility  $\mathcal{V}_A$  analogous to (6), one gets

$$\langle \mathcal{J}_B \rangle_t = 6\alpha_A \lambda_A^2 = \frac{3\nu_A}{8(\nu_A + 1)} \frac{\mathcal{V}_A^2}{v_L^2(\phi_A)} \quad (19)$$

with errors of order  $\lambda_A^3$ . We see that  $\langle \mathcal{J}_B \rangle_t$  is independent of the initial coherence, number of atoms, and Peierls phase of the gas  $B$  and of the size  $L$  of the ring. Moreover, it depends quadratically on the initial



visibility of the gas  $A$ . Recalling that  $v_L(\phi_A) \rightarrow 1$  for  $L \rightarrow \infty$ , the dependence on the Peierls phase  $\phi_A$  of the expression in the last member of Eq. (19) disappears in the infinite size limit.

Comparing Eq. (19) with the numerical results shown in Fig. 3(a), which displays  $\langle \mathcal{J}_B \rangle_t / \mathcal{V}_A^2$  as function of  $\mathcal{V}_A$  for two different values of  $\lambda_B$  corresponding to the gas  $B$  being initially in the MI and SF regimes and for different phases, a good agreement is observed when  $\mathcal{V}_A \ll 1$ , the values calculated numerically being about 5% above the prediction of Eq. (19). Clear deviations from Eq. (19) show up for  $\mathcal{V}_A \gtrsim 0.2$ , as expected from the fact that this equation is valid for  $\lambda_A \ll 1$  only. However, Fig. 3(b) shows that for such visibilities these deviations become smaller by increasing the lattice size.

The physical origin of the reduction of the  $B$ -current when the two gases are coupled at time  $t > 0$  can be understood by looking at the effect on the  $B$ -atoms of particle-hole excitations in the gas  $A$  (Note that the MI state of the gas  $A$  has no effect on the  $B$ -current since the attractive potential produced on each  $B$ -atom by its coupling with the gas  $A$  in the MI state is site-independent and equal to  $-V\nu_A$ ; in other words, if the two gases are in the state  $|\psi_{\text{MI}}\rangle|\psi_B\rangle$  then their coupling energy is independent of the distribution of the  $B$ -atoms on the lattice and is equal to  $-V\nu_A N_B$ , as noted in Sec. 2.) Consider e.g. a gas  $A$  in the particle-hole state  $|\varphi_{A,j,+}\rangle$ . Then the transfer of a  $B$ -atom from site  $j+1$  to site  $j$  has a coupling energy cost of  $2V$  (in fact, the coupling energy increases by  $V(\nu_A+1)$  when removing the  $B$ -atom from site  $j+1$  and decreases by  $V(\nu_A-1)$  when adding it on site  $j$ ). Similarly, if the gas  $A$  is in the particle-hole state  $|\varphi_{A,j,-}\rangle$ , the transfer of a  $B$ -atom from site  $j$  to site  $j+1$  has an energy cost of  $2V$ . We can infer that particle-hole excitations in the gas  $A$  slow down the flow of  $B$ -atoms in the ring lattice. We shall come back to this effect in Sect. 6 after having studied the entanglement generation between the two gases.

## 5 Interspecies entanglement and its relation with the $B$ -current

The reduction of current is due to quantum correlations between the  $A$ - and  $B$ -atoms induced by the interspecies coupling. We estimate the amount of entanglement between the two gases using the shifted Schmidt number

$$\mathcal{K}_{AB}(t) = (\text{tr}_A[\hat{\rho}_A^2(t)])^{-1} - 1 = (\text{tr}_B[\hat{\rho}_B^2(t)])^{-1} - 1, \quad (20)$$

where  $\hat{\rho}_A(t) = \text{tr}_B |\psi_{AB}(t)\rangle\langle\psi_{AB}(t)|$  is the reduced density matrix of the gas  $A$  at time  $t$ . The shift by one in our definition of the Schmidt number, as compared with the usual definition, makes sure that  $\mathcal{K}_{AB}(t) = 0$  when the two gases are unentangled. Note that  $\mathcal{K}_{AB}(t)$  is symmetric under the exchange of  $A$  and  $B$ .

Assuming as before that the gas  $A$  is in the MI regime and considering times  $t$  much smaller than  $U_A^{-1}$ , a simple calculation using the perturbative expansion (12) and neglecting the hopping of atoms  $A$  in the dynamics yields (see in Appendix B)

$$\mathcal{K}_{AB}(t) = 4L\alpha_A\lambda_A^2 \left(1 - \left|\langle e^{-it\hat{W}_B^{(01)}} \rangle_{\psi_B}\right|^2\right) + \mathcal{O}(\lambda_A^3) \quad (21)$$

with the Hamiltonian

$$\hat{W}_B^{(01)} = \hat{H}_B - V\Delta\hat{n}_{01}^B, \quad \Delta\hat{n}_{01}^B = \hat{n}_1^B - \hat{n}_0^B. \quad (22)$$

In this section, like for the calculation of the  $B$ -current, we restrict our analysis to times  $t$  much smaller than all the inverse single species energies. We refer to this condition as defining the *short time regime*. The behavior of the Schmidt number at larger times will be discussed in Sec. 7. By applying (21), we first determine  $\mathcal{K}_{AB}(t)$  in the short time regime in two limits:  $\lambda_B \ll 1$  (gas  $B$  in the MI regime) in Subsect. 5.1 and  $\lambda_B \gg 1$  (gas  $B$  in the SF regime) in Subsect. 5.2. We then discuss the general case in Subsect. 5.3.

## 5.1 Gases $A$ and $B$ in the MI regime

Let us first assume that both gases are in the MI regime ( $\lambda_A, \lambda_B \ll 1$ ). For times  $t \ll U_A^{-1}, U_B^{-1}$ , the Hamiltonian  $\hat{H}_B$  can be replaced by  $\hat{H}_B^{\text{int}}$  in Eq. (21) and thus be dropped out (recall that  $[\hat{H}_B^{\text{int}}, \Delta \hat{n}_{01}^B] = 0$  and  $\hat{H}_B |\psi_B\rangle = E_{\text{GS}}^B |\psi_B\rangle$ ). The quantum expectation in this equation becomes the same as in the calculation of the  $B$ -current, replacing  $A$  by  $B$ . This yields

$$\mathcal{K}_{AB}(t) = 16L\alpha_A\alpha_B\lambda_A^2\lambda_B^2[3 - 2\cos(tV) - \cos(2tV) + \mathcal{O}(\lambda_A) + \mathcal{O}(\lambda_B)] \quad (23)$$

with  $\alpha_B = \nu_B(\nu_B + 1)$ . Averaging up to time  $t$  with  $V^{-1} \ll t \ll U_A^{-1}, U_B^{-1}$  one gets

$$\langle \mathcal{K}_{AB} \rangle_t = 48L\alpha_A\alpha_B\lambda_A^2\lambda_B^2 = \frac{3L}{16} \frac{\nu_A\nu_B}{(\nu_A + 1)(\nu_B + 1)} \frac{\mathcal{V}_A^2 \mathcal{V}_B^2}{v_L(\phi_A)^2 v_L(\phi_B)^2}, \quad (24)$$

where we have used in the last equality the linear approximation of the visibility, see (6).

In Eqs. (23) and (24) we can observe that the shifted Schmidt number is proportional to the system size  $L$ . Note that the 2-Rényi entropy of entanglement, which is a meaningful entanglement measure analogous to the entanglement of formation [57], is related to the Schmidt number defined in (20) by

$$S_{AB}^{(2)}(t) = \ln(\mathcal{K}_{AB}(t) + 1) \simeq \mathcal{K}_{AB}(t), \quad (25)$$

where the second equality holds for  $\mathcal{K}_{AB}(t) \ll 1$ . The latter condition is satisfied for not too large  $L$ 's in Eq. (24) since we assume  $\lambda_A, \lambda_B \ll 1$ . Therefore, the entanglement entropy after the quench scales linearly with the system size  $L$ .

Furthermore, by comparing (19) and (23) one finds that  $\mathcal{K}_{AB}(t)$  (and thus  $S_{AB}^{(2)}(t)$ ) is proportional to the relative  $B$ -current reduction,

$$S_{AB}^{(2)}(t)/L = \mathcal{K}_{AB}(t)/L = \beta_{\nu_B, \lambda_B} \mathcal{J}_B(t) \quad (26)$$

with a proportionality factor  $\beta_{\nu_B, \lambda_B} = 8\alpha_B\lambda_B^2$  depending on the filling factor  $\nu_B$  and the energy ratio  $\lambda_B$  of the  $B$ -gas only. Using (6) again, one has

$$\beta_{\nu_B, \lambda_B} = 8\alpha_B\lambda_B^2 = \frac{\nu_B}{2\nu_B + 2} \frac{\mathcal{V}_B^2}{v_L^2(\phi_B)}, \quad (27)$$

showing that  $\mathcal{K}_{AB}(t)/L$  is proportional to  $\mathcal{V}_B^2 \mathcal{J}_B(t)$ .

It is worth noting that the time-averaged Schmidt number per site has a universal value  $48\alpha_A\alpha_B\lambda_A^2\lambda_B^2$ , see (24), which is independent of the Peierls phases and, more remarkably, of the strength  $V$  of the inter-species interactions. Moreover, the amplitude of the time oscillations of  $\mathcal{K}_{AB}(t)$  has also a universal character, see (23); in particular it does not depend on  $V$  which only sets in the period of oscillations.

Since both the  $B$ -current and the visibilities are measurable quantities, Eqs. (24) and (26) provide a way to evaluate the amount of  $A$ - $B$  entanglement. This can be done either by measuring the interference patterns of the two gases prior to the interaction quench (Eq. (24)) or by performing measurements prior and after the quench on the gas  $B$  only (Eq. (26)). Note that the usual technique to estimate entanglement experimentally in quantum many-body systems relies on quantum state tomography (see [69, 70] and references therein) and can be applied in practice to small systems only (see also alternative techniques proposed in [43, 59, 60, 61]). In contrast, estimating entanglement from observations of the interference patterns and measurement of the atomic current can be done without any restriction on the system size.

The numerical results displayed in Fig. 4 show good agreement with Eqs. (24) and (26) for values of  $\lambda_A$  corresponding to  $\mathcal{V}_A \lesssim 0.2$ . For higher visibilities  $\mathcal{V}_A$ , it is seen in the left panel that  $\langle \mathcal{K}_{AB} \rangle_t$  depends on the Peierls phases. Note that for large  $L$ , (26 and (27) give  $\langle \mathcal{K}_{AB} \rangle_t/L = (\nu_B/(2\nu_B + 2))\mathcal{V}_B^2 \langle \mathcal{J}_B \rangle_t$ , hence the slopes of the straight lines in the right panel become  $\phi_A$ -independent and equal to  $1/4$ .

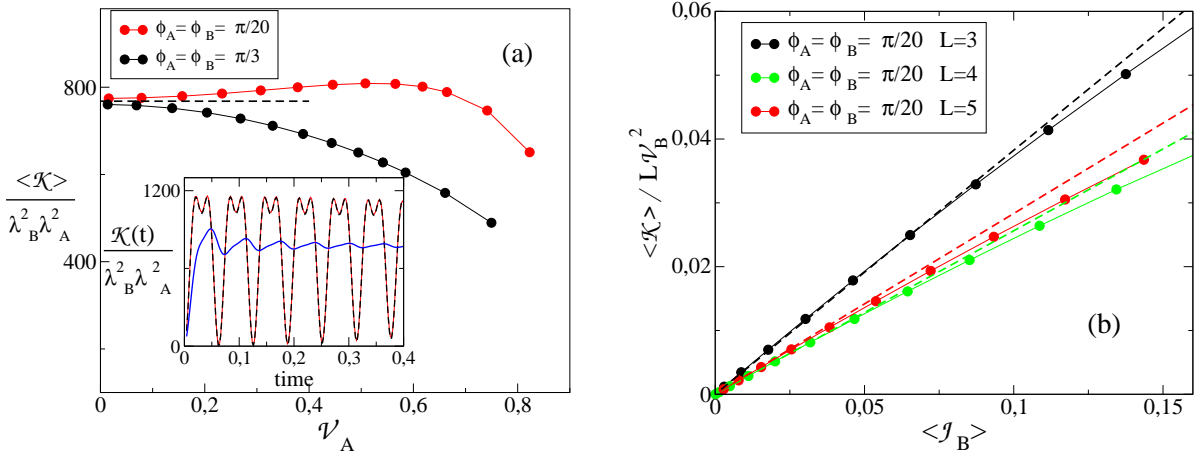


Figure 4: **(a):** Time averaged Schmidt number  $\langle \mathcal{K}_{AB} \rangle_t$  divided by  $\lambda_A^2 \lambda_B^2$  vs. initial visibility of the gas  $A$  for a gas  $B$  in the MI regime. The parameters are  $L = N_A = N_B = 4$ ,  $V = 100U_B$ ,  $J_B = 0.02U_B$ ,  $U_A = 0.1U_B$ ,  $J_A$  variable,  $\phi_A = \phi_B = \pi/20$  (red dots) and  $\pi/3$  (black dots), averaging time  $t = 0.3/U_B$ . Horizontal dashed segment: value of Eq. (24). **Inset:** Schmidt number vs time (in units of  $U_B^{-1}$ ) for the same parameters and  $J_A = 0.0002U_B$ . Red and blue line:  $\mathcal{K}_{AB}(t)$  and  $\langle \mathcal{K}_{AB} \rangle_t$  from numerical calculations. Dashed black lines: formula (64). **(b):**  $\langle \mathcal{K}_{AB} \rangle_t / L$  divided by the squared visibility of the gas  $B$  vs. relative current reduction  $\langle \mathcal{J}_B \rangle_t$ , for the same energy parameters,  $\phi_A = \phi_B = \pi/20$ , and  $L = N_A = N_B = 3, 4$  and  $5$  (black, green, and red points). Dashed lines: values from Eqs. (26) and (27).

## 5.2 Gases $A$ and $B$ in the MI and SF regime

Let us now assume that the gases  $A$  and  $B$  are in the MI and SF regimes, respectively ( $\lambda_A \ll 1 \ll \lambda_B$ ). We will show that, after averaging over time, the shifted Schmidt number and 2-Rényi entropy of entanglement show again a linear growth with the system size  $L$  and a proportionality to the relative (time-averaged)  $B$ -current reduction,

$$\langle S_{AB}^{(2)} \rangle_t / L = \langle \mathcal{K}_{AB} \rangle_t / L = \beta_{\nu_B, \infty} \langle \mathcal{J}_B \rangle_t \quad (28)$$

with  $\beta_{\nu_B, \infty}$  depending on the filling factor  $\nu_B$  and being almost independent of  $L$ . For instance, for  $\nu_B = 1$  one has  $\beta_{\nu_B, \infty} = 0.53 \pm 0.01$  with a difference between the values for  $L = 3, 4, 5$ , or  $L \rightarrow \infty$  smaller than 0.01 (see Table 1). To prove (28), we assume that the Peierls phase  $\phi_B$  is not close to a half-integer value of  $\phi_0$  and approximate the GS  $|\psi_B\rangle$  of the gas  $B$  by the SF state

$$|\psi_{\text{SF}}\rangle = \frac{1}{\sqrt{L^{N_B} N_B!}} \left( \sum_{j=0}^{L-1} e^{i\phi_0 \ell j} b_j^\dagger \right)^{N_B} |0\rangle = \sqrt{\frac{N_B!}{L^{N_B}}} \sum_{\underline{n}} \frac{e^{i\phi_0 \ell \sum_j j n_j}}{\sqrt{n_0! \dots n_{L-1}!}} |\underline{n}\rangle \quad (29)$$

(here  $|0\rangle$  denotes the vacuum state), making a small error  $\mathcal{O}(\lambda_B^{-1})$ . As mentioned above, in the short time regime  $t \ll J_B^{-1}, U_A^{-1}$  one may replace  $\hat{W}_B^{(01)}$  by  $-V \Delta \hat{n}_{01}^B$  in the quantum expectation in (21), which

$L$	$\nu_B$	$\beta_{\nu_B,\infty}$ (small time regime)	$\beta'_{\nu_B,\infty}$ (intermediate time regime)
3	1	$\frac{392}{729} \simeq 0.5377$	
4	1	$\frac{26333}{49152} \simeq 0.5357$	
5	1	$\simeq 0.5344$	
$\infty$	1	$\simeq 0.5287$	$\simeq 0.6032$
3	2	$\simeq 0.5741$	
$\infty$	2	$\simeq 0.5710$	$\simeq 0.6381$

Table 1: Proportionality factors  $\beta_{\nu_B,\infty}$  of Eq. (28) and  $\beta'_{\nu_B,\infty}$  of Eq. (74) when the gas  $B$  is in the SF regime for some values of the site number  $L$  and filling factor  $\nu_B$ .

becomes

$$\begin{aligned}
\langle e^{-it\hat{W}_B^{(01)}} \rangle_{\psi_B} &= \sum_{\underline{n}} e^{itV(n_1-n_0)} |\langle \underline{n} | \psi_{\text{SF}} \rangle|^2 + \mathcal{O}(\lambda_B^{-1}) \\
&= \frac{N_B!}{L^{N_B}} \sum_{\sigma=0}^{N_B} \left( \sum_{n_0+n_1=\sigma} \frac{e^{itVn_1} e^{-itVn_0}}{n_0!n_1!} \right) \sum_{\underline{n}'}^{(\sigma)} \frac{1}{n_2'! \cdots n_{L-1}'!} + \mathcal{O}(\lambda_B^{-1}) \\
&= \sum_{\sigma=0}^{N_B} \frac{1}{L^\sigma} \left( 2 \cos(tV) \right)^\sigma \frac{N_B!}{\sigma!(N_B-\sigma)!} \left( \frac{L-2}{L} \right)^{N_B-\sigma} + \mathcal{O}(\lambda_B^{-1}). \tag{30}
\end{aligned}$$

Here, the sum over  $\underline{n}'$  in the second line runs over all  $(L-2)$ -dimensional vectors  $\underline{n}' = (n_2', \dots, n_{L-1}') \in \mathbb{N}^{L-2}$  such that  $\sum_{j=2}^{L-1} n_j' = N_B - \sigma$ , and in the last line we have used the multinomial formula

$$\left( \sum_{j \in \mathcal{J}} x_j \right)^N = N! \sum_{\sum_j n_j = N, n_j \geq 0} \prod_{j \in \mathcal{J}} \frac{x_j^{n_j}}{n_j!} \quad \text{if } \mathcal{J} \subset \mathbb{N} \text{ is a finite subset of indices and } x_j \in \mathbb{R}.$$

Plugging (30) into (21), this yields

$$\frac{\mathcal{K}_{AB}(t)}{L} = 4\alpha_A \lambda_A^2 \left\{ 1 - \left( 1 - \frac{2}{L} (1 - \cos(tV)) \right)^{2N_B} + \mathcal{O}(\lambda_A) + \mathcal{O}(\lambda_B^{-1}) \right\}. \tag{31}$$

Averaging over a time interval  $[0, t]$  with  $t \gg V^{-1}$  and using Eq. (19), one obtains Eq. (28) above with the proportionality factor

$$\beta_{\nu_B,\infty} = \frac{2}{3} \left\{ 1 - \frac{1}{2\pi} \int_0^{2\pi} ds \left( 1 - \frac{2}{L} (1 - \cos s) \right)^{2N_B} \right\} \sim \frac{2}{3} \left\{ 1 - \frac{1}{2\pi} \int_0^{2\pi} ds e^{-4\nu_B(1-\cos s)} \right\}, \tag{32}$$

where the last expression corresponds to the thermodynamical limit  $N_B, L \gg 1$  with a fixed  $\nu_B = N_B/L$ . The values of  $\beta_{\nu_B,\infty}$  for  $N_B = 3, 4$ , and  $5$  and  $\nu_B = 1$  or  $2$  are given in Table 1. It is noteworthy that they coincide with the value at the thermodynamical limit up to the second decimal.

The time evolution of the Schmidt number determined numerically when the gas  $B$  is in the SF regime is shown in Figs. 5(a) and (b). One sees that  $\mathcal{K}_{AB}(t)$  presents, in addition to oscillations of period  $2\pi/V$ , a complex behavior which is likely to result from the superposition of the different frequencies associated to the energy parameters  $U_A, U_B$ , and  $J_B$  entering the Bose-Hubbard Hamiltonians. Nonetheless, the time-averaged Schmidt number  $\langle \mathcal{K}_{AB} \rangle_t$  has a much simpler evolution and basically displays two plateaus. The first plateau at small time  $t \lesssim J_B^{-1}$  agrees well with the predicted value obtained by replacing  $\langle \mathcal{J}_B \rangle_t$  by

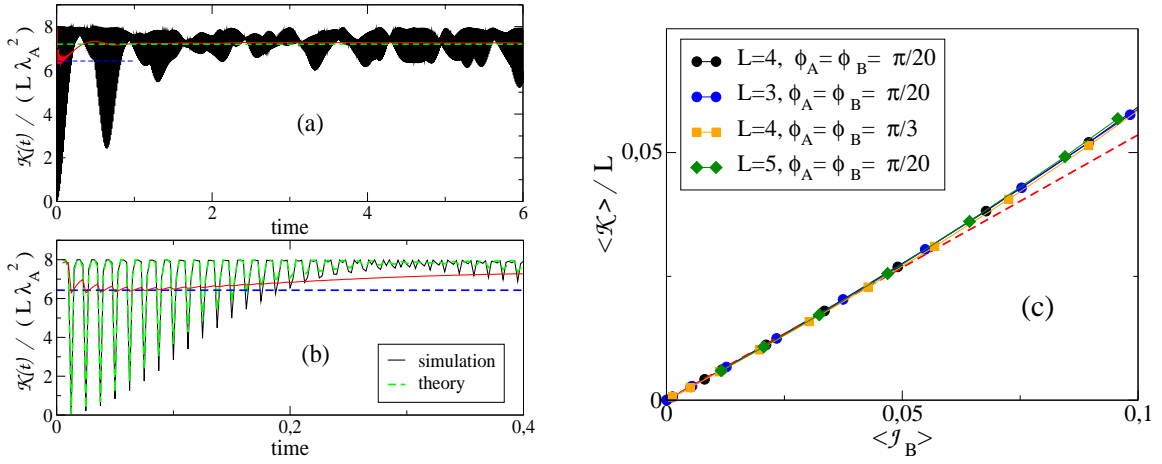


Figure 5: **(a)**: Schmidt number  $\mathcal{K}_{AB}(t)$  divided by  $L\lambda_A^2$  vs. time (black plain line) and its time average  $\langle \mathcal{K}_{AB} \rangle_t / (L\lambda_A^2)$  (red plain line) for a gas  $B$  in the SF regime. Time is in units of  $U_B^{-1}$ . The parameters are  $L = N_A = N_B = 4$ ,  $V = 500U_B$ ,  $J_B = 5U_B$ ,  $U_A = 0.1U_B$ ,  $J_A = 0.002U_B$ , and  $\phi_A = \phi_B = \pi/3$ . The blue and green dashed horizontal lines display the time averaged values from Eq. (75) in the short and intermediate time regimes, respectively. **(b)**: same on the time interval  $[0, 0.4/U_B]$  with formula (73) shown in green dashed lines. **(c)**: Time-averaged Schmidt number per site  $\langle \mathcal{K}_{AB} \rangle_t / L$  vs. relative current reduction  $\langle J_B \rangle_t$ , for  $N_A = N_B = L$  and  $\phi_A = \phi_B = \phi$  with  $L = 3$ ,  $\phi = \pi/20$  (blue dots),  $L = 4$ ,  $\phi = \pi/20$  (black dots),  $L = 4$ ,  $\phi = \pi/3$  (orange squares), and  $L = 5$ ,  $\phi = \pi/20$  (green diamonds). The energy parameters are  $U_A = 0.1U_B$ ,  $J_B = U_B$ ,  $J_A$  variable, averaging time  $t = 0.3/U_B$ . Dashed line: values from Eqs. (28) with  $\beta_{\nu_B, \infty} = 0.54$  (see Table 1).

$6\alpha_A\lambda_A^2$  in Eq. (28) (blue dashed line). We shall derive in Sec. 7 an analytical formula giving the value of the second plateau at times  $t \gtrsim J_B^{-1}$  in the limit  $L \rightarrow \infty$  (see Eq. (75) below). The fact that this formula reproduces well the value of the second plateau for  $L = 4$  in Fig. 5(a) is an indication that the time-averaged Schmidt number is not sensitive to finite size effects. In Fig. 5(c) one observes that  $\langle \mathcal{K}_{AB} \rangle / L$  is proportional to  $\langle J_B \rangle$  for small values of  $\langle J_B \rangle$ , i.e., small values of  $\lambda_A$ , with a proportionality factor in very good agreement with the predicted value  $\beta_{\nu_B, \infty}$  in Eq. (28). Interestingly, although  $\langle \mathcal{K}_{AB} \rangle / L$  is seen to behave non-linearly with  $\langle J_B \rangle$  at larger  $\langle J_B \rangle$ 's, the curves obtained for  $L = 3$ ,  $L = 4$ , and  $L = 5$  are superposed on each others, suggesting once again that finite size effects are not relevant.

Note that our calculations of the  $B$ -current and Schmidt number in the previous and in this section are restricted to times much smaller than the inverse single species energies (small time regime). In the thermodynamical limit, since these energies scale linearly with the atom numbers  $N_A$  and  $N_B$ , to insure the validity of our results up to finite times  $t > 0$  one must a priori re-scale the energy parameters in the Bose-Hubbard Hamiltonians  $\hat{H}_A$  and  $\hat{H}_B$  as  $U_A \rightarrow U_A/N_A$ ,  $J_A \rightarrow J_A/N_A$ ,  $U_B \rightarrow U_B/N_B$  and  $J_B \rightarrow J_B/N_B$ .

We will extend in Sec.7 the above results on the Schmidt number in both the MI regime  $\lambda_B \ll 1$  and the SF regime  $\lambda_B \gg 1$  to larger times of order  $U_B^{-1}$  and  $J_B^{-1}$ , respectively, keeping the assumption  $t$  much smaller than the inverse interaction energy of the  $A$ -atoms. It will be shown that the time-averaged Schmidt number is still given at these larger times by Eqs. (24) in the MI regime and by Eq. (28) with a slightly different prefactor  $\beta_{\nu_B, \infty}$  in the SF regime.

### 5.3 Gas $A$ in the MI regime, $\lambda_B$ arbitrary

In the more general case  $\lambda_B$  arbitrary and  $\lambda_A \ll 1$ , one deduces from (21) and (19) that

$$\langle \mathcal{K}_{AB} \rangle_t / L = \beta_{\nu_B, \lambda_B, L} \langle \mathcal{J}_B \rangle_t \quad , \quad V^{-1} \ll t \ll U_A^{-1}, U_B^{-1}, J_B^{-1} \quad , \quad (33)$$

with a proportionality factor given by

$$\beta_{\nu_B, \lambda_B, L} = \frac{2}{3} \left( 1 - \frac{1}{2\pi} \int_0^{2\pi} ds |\langle e^{is\Delta\hat{n}_{01}^B} \rangle_{\psi_B}|^2 \right) = \frac{2}{3} \left( 1 - \sum_{\underline{n}, \underline{m}, n_1 - n_0 = m_1 - m_0} |\langle \underline{n} | \psi_B \rangle|^2 |\langle \underline{m} | \psi_B \rangle|^2 \right) . \quad (34)$$

Note that  $|\psi_B\rangle$  and thus  $\beta_{\nu_B, \lambda_B, L}$  depend on  $L$ , so that we cannot claim that Eq. (33) shows a linear growth of entanglement with the system size for finite lattices and  $\lambda_B \approx 1$ , although one may expect that  $\beta_{\nu_B, \lambda_B, L}$  converges rapidly to its large  $L$  limiting value as in the case  $\lambda_B \gg 1$ .

Since only observables and quantum expectations of the gas  $B$  appear in the RHS of Eq. (33), this equation provides a way to estimate the amount of entanglement between the two gases when  $\lambda_A \ll 1$  by *performing local measurements on the species  $B$* .

## 6 Quantum superpositions at the origin of the entanglement

In order to understand better the entanglement generation process in the quench dynamics, it is enlightening to look at the superpositions at the origin of this entanglement in the time-evolved wavefunction of the two gases. With this aim, we determine this wavefunction  $|\psi_{AB}(t)\rangle$  to second order in  $\lambda_A$ .

Disregarding as before the tunneling Hamiltonian  $\hat{K}_A$  and the commutator  $[\hat{H}_{AB}^{\text{int}}, \hat{H}_B]$  in the dynamical evolution up to times  $t \ll U_A^{-1}, U_B^{-1}, J_B^{-1}$  and recalling that  $\hat{H}_B |\psi_B\rangle = E_{\text{GS}}^B |\psi_B\rangle$ , we find from (2) and (12)

$$|\psi_{AB}(t)\rangle = e^{-it\hat{H}_{AB}^{\text{int}}} e^{-it\hat{H}_A^{\text{int}}} e^{-itE_{\text{GS}}^B} (|\psi_{\text{MI}}\rangle + \lambda_A |\psi_A^{(1)}\rangle + \lambda_A^2 |\psi_A^{(2)}\rangle + \mathcal{O}(\lambda_A^3)) |\psi_B\rangle . \quad (35)$$

Let us expand the initial GS of  $B$  in the Fock basis as  $|\psi_B\rangle = \sum_{\underline{n}_B} c_{\underline{n}_B} |\underline{n}_B\rangle$  and separate the second-order correction to the GS of  $A$  as the sum of  $\langle \psi_{\text{MI}} | \psi_A^{(2)} \rangle |\psi_{\text{MI}}\rangle$  and  $\Pi_{\text{MI}}^\perp |\psi_A^{(2)}\rangle$ , where  $\Pi_{\text{MI}}^\perp = 1 - |\psi_{\text{MI}}\rangle \langle \psi_{\text{MI}}|$  is the projector onto the orthogonal subspace to the MI state. Using (13) and (14) and recalling that the energy to create a particle-hole excitation is equal to  $U_A$ , we obtain

$$\begin{aligned} |\psi_{AB}(t)\rangle &= e^{-it(V\nu_A N_B + E_A^{(0)}(\nu_A) + E_{\text{GS}}^B)} \left\{ (1 - \lambda_A^2 \alpha_A L) |\psi_{\text{MI}}\rangle |\psi_B\rangle \right. \\ &\quad + \lambda_A \sqrt{\alpha_A} e^{-itU_A} \sum_j \sum_{\underline{n}_B} c_{\underline{n}_B} \left( e^{i\phi_A} e^{-itV(n_{j+1}^B - n_j^B)} |\varphi_{A,j,+}\rangle + e^{-i\phi_A} e^{itV(n_{j+1}^B - n_j^B)} |\varphi_{A,j,-}\rangle \right) |\underline{n}_B\rangle \Big\} \\ &\quad + \lambda_A^2 e^{-itE_{\text{GS}}^B} e^{-it\hat{H}_{AB}^{\text{int}}} e^{-it\hat{H}_A^{\text{int}}} \Pi_{\text{MI}}^\perp |\psi_A^{(2)}\rangle |\psi_B\rangle + \mathcal{O}(\lambda_A^3) , \end{aligned} \quad (36)$$

where  $|\varphi_{A,j,\pm}\rangle$  are the particle-hole states, see 16. It is easy to convince oneself that the contribution of the term in the last line of (36) to the reduced density matrix  $\hat{\rho}_B(t) = \text{tr}_A |\psi_{AB}(t)\rangle \langle \psi_{AB}(t)|$  of the gas  $B$  is of order  $\lambda_A^3$  or higher. Since we are interested in the Schmidt number and the  $B$ -current, which both depend on  $\hat{\rho}_B(t)$  only (see (20) and (9)), this term can be dropped out. Disregarding also the irrelevant phase factor, the wavefunction of the two gases at time  $t$  is given by

$$(1 - \lambda_A^2 \alpha_A L) |\psi_{\text{MI}}\rangle |\psi_B\rangle + \lambda_A \sqrt{\alpha_A} e^{-itU_A} \sum_{j,\pm} e^{\pm i\phi_A} |\varphi_{A,j,\pm}\rangle |\psi_{B,j,\pm}(t)\rangle + \mathcal{O}(\lambda_A^3) \quad (37)$$

with

$$|\psi_{B,j,\pm}(t)\rangle = \sum_{\underline{n}_B} c_{\underline{n}_B} e^{\mp itV(n_{j+1}^B - n_j^B)} |\underline{n}_B\rangle . \quad (38)$$

The corrections of order  $\lambda_A$  to the separable state  $|\psi_{\text{MI}}\rangle|\psi_B\rangle$  in (37) are at the origin of the entanglement between the two gases. Thus entanglement comes from the coupling of particle-hole excitations  $|\varphi_{A,j,\pm}\rangle$  in the gas  $A$  with the states  $|\psi_{B,j,\pm}(t)\rangle$  of the gas  $B$  at each lattice site  $j$ . Let us note that the latter states are periodic in time with period  $2\pi/V$ ; in particular, they come back to their initial  $j$ -independent value  $|\psi_B\rangle$  at times  $t_m = 2m\pi/V$ ,  $m = 1, 2, \dots$ , leading to a disappearance of entanglement (this is valid when  $t_m \ll U_A^{-1}, U_B^{-1}, J_B^{-1}$ ; see the next section for larger times). This explains the observed oscillations of  $\mathcal{K}_{AB}(t)$  with period  $2\pi/V$  in the inset of Fig. 4(a) and in Fig. 5(b).

We now look at the effect of the aforementioned superpositions on the  $B$ -current  $I_B(t) = \text{tr}_B[\hat{\rho}_B(t)\hat{I}_B]$ . Plugging into this formula the reduced density matrix  $\hat{\rho}_B(t)$  obtained from the wavefunction 37, one gets

$$I_B(t) = (1 - 2\lambda_A^2\alpha_A L)I_B(0) + \lambda_A^2\alpha_A \sum_{j,\pm} \langle \hat{I}_B \rangle_{\psi_{B,j,\pm}(t)} + \mathcal{O}(\lambda_A^3). \quad (39)$$

The reduction of the  $B$ -current comes from the fact that the currents  $\langle \hat{I}_B \rangle_{\psi_{B,j,\pm}(t)}$  in the states  $|\psi_{B,j,\pm}(t)\rangle$  are smaller than  $I_B(0)$ . In fact, a simple calculation shows that these currents averaged in the time interval  $[0, t]$  with  $t \gg 1/V$  are equal to

$$\langle \langle \hat{I}_B \rangle_{\psi_{B,j,\pm}} \rangle_t = \frac{1}{2iL} \sum_{i \notin \{j-1, j, j+1\}} \langle \psi_B | (e^{i\phi_B} \hat{b}_{i+1}^\dagger \hat{b}_i - \text{h.c.}) | \psi_B \rangle. \quad (40)$$

This expression is nothing but the current for the initial state  $|\psi_B\rangle$  in the ring after having removed the three sites  $i = j-1, j$ , and  $j+1$ . Replacing  $\langle \hat{I}_B \rangle_{\psi_{B,j,\pm}(t)}$  by  $(L-3)I_B(0)/L$  in (39), one gets back formula (19) for the relative current variation. We conclude that the universal reduction of  $B$ -current is due to the coupling of particle-hole excitations in the gas  $A$  with the states (38) of the  $B$ -gas. The latter have a time-averaged current reduced by a factor  $(L-3)/L$ , in qualitative agreement with the intuitive energetic argument given in Sec. 4.

Let us stress that as a consequence of the energy scale separation (3), all states appearing in the wavefunction (37) have energies much higher than the GS energy  $E_{AB}^{\text{GS}} \approx -V N_A N_B$  for the post-quench Hamiltonian  $\hat{H}_{AB}$ . More precisely,

$$\begin{aligned} \langle \hat{H}_{AB} \rangle_{\psi_{\text{MI}} \otimes \psi_B} &\equiv -V\nu_A N_B + E_A^{(0)}(\underline{\nu}_A) + E_{\text{GS}}^B + \mathcal{O}(J_A) \\ \langle \hat{H}_{AB} \rangle_{\varphi_{A,j,\pm} \otimes \psi_{B,j,\pm}(t)} &= -V\nu_A N_B - V \langle \hat{n}_{j+1}^B - \hat{n}_j^B \rangle_{\psi_B} + E_A^{(0)}(\underline{\nu}_A) + U_A + \langle \hat{H}_B \rangle_{\psi_{B,j,\pm}(t)} + \mathcal{O}(J_A). \end{aligned} \quad (41)$$

In particular, the GS of the post-quench Hamiltonian  $\hat{H}_{AB}$  does not play any role in the quench dynamics at the times we are considering. This can be explained from the fact that the initial state  $|\psi_A\rangle|\psi_B\rangle$  has an energy lying in the highly excited part of the spectrum of  $\hat{H}_{AB}$ . This is illustrated in the numerical results of Fig. 6 displaying the probabilities  $p_i = |\langle \psi_{AB}(t) | \Phi_i \rangle|^2$  of finding the wavefunction of the two gases in the eigenstates  $|\Phi_i\rangle$  of  $\hat{H}_{AB}$  (note that the  $p_i$  are time independent). The peak with value  $p_i^*$  close to 1 corresponds to the eigenstate of  $\hat{H}_{AB}$  with closest eigenvalue to  $E_{AB}^{(0)*} = -V\nu_A N_B + E_A^{(0)}(\underline{\nu}_A) + E_{\text{GS}}^B$ . Actually, the state  $|\psi_{\text{MI}}\rangle|\psi_B\rangle$  in (37) is an eigenstate of  $\hat{H}_{AB}^{(0)} = \hat{H}_A^{\text{int}} + \hat{H}_B + \hat{H}_{AB}^{\text{int}}$  with eigenvalue  $E_{AB}^{(0)*}$ . Thus by perturbation theory  $\hat{H}_{AB} = \hat{H}_{AB}^{(0)} + \hat{K}_A$  has an eigenvector  $|\Phi_{AB}^*\rangle$  differing from this state by  $\mathcal{O}(J_A/V)$  with eigenenergy  $E_{AB}^* = E_{AB}^{(0)*} + \mathcal{O}(J_A)$ . The corresponding probability  $p_i^*$  is the square of the coefficient multiplying  $|\psi_{\text{MI}}\rangle|\psi_B\rangle$  in (37),

$$p_i^* = |\langle \psi_{\text{MI}} | \langle \psi_B | \psi_{AB}(t) \rangle + \mathcal{O}(J_A/V) |^2 = 1 - 2\lambda_A^2\alpha_A L + \mathcal{O}(\lambda_A^3) + \mathcal{O}(J_A/V). \quad (42)$$

The small non-zero probabilities shown in the two insets are the contribution of the linear terms in (37), which are at the origin of the entanglement. The peak in the upper inset comes from the time-independent contribution in these linear terms obtained by forgetting all Fock states with  $n_j^B \neq n_{j+1}^B$  in the definition (38) of  $|\psi_{B,j,\pm}(t)\rangle$ ; such states have inter-species interaction energy  $-V\nu_A N_B$  and contribute to the time-averaged current.

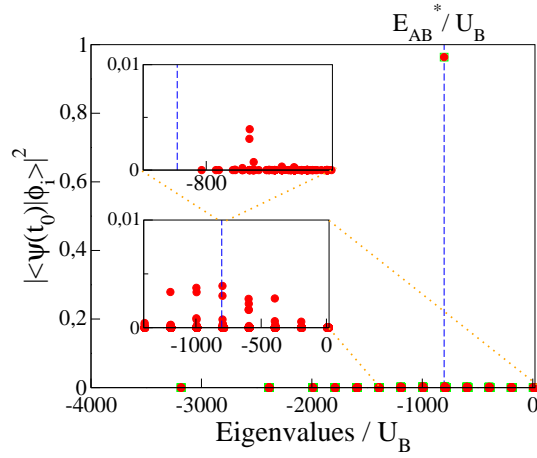


Figure 6: Probabilities  $p_i = |\langle \psi_{AB}(t_0) | \Phi_i \rangle|^2$  of finding the wavefunction of the two gases at time  $t_0$  in an eigenstate  $|\Phi_i\rangle$  of the post-quench Hamiltonian  $\hat{H}_{AB}$ , for  $N_A = N_B = L = 4$ ,  $V = 200U_B$ ,  $J_B = U_A = U_B$ ,  $J_A = 0.05U_B$ ,  $\phi_A = \phi_B = \pi/10$ , and  $t_0 = 1/U_B$  (from numerical exact diagonalization). We checked that the numerically evaluated values of  $p_i$  do not change when changing  $t_0$ , as it should be. Each red point corresponds to a given eigenstate of  $\hat{H}_{AB}$  with an eigenenergy  $E_{AB}^i$  represented in the horizontal axis (in units of  $U_B$ ) and the associated probability  $p_i$  represented in the vertical axis. The eigenenergy  $E_{AB}^*$  at which  $p_i$  displays a maximum is defined in the text. The insets show amplifications in particular regions of the spectrum. For energies  $E_{AB}^i \lesssim -1600U_B$  the values of  $p_i$  are smaller than  $2 \times 10^{-5}$ .

## 7 Interspecies entanglement at larger times

In this section, we determine the Schmidt number at times  $t$  that can be of order  $U_B^{-1}$  or  $J_B^{-1}$  but must be small with respect to the inverse interaction energy of the gas  $A$ , i.e.,

$$0 \leq t \ll (N_A U_A)^{-1}. \quad (43)$$

Having in mind that the interaction energy of the gas  $A$  can be tuned to be smaller than  $U_B$  and  $J_B$  (this can be done experimentally using Feshbach resonances or by varying the atom number  $N_A$ ), we define an *intermediate time regime* by  $U_B^{-1}, J_B^{-1} \lesssim t \ll (N_A U_A)^{-1}$ . Note that one may exchange the role of  $A$  and  $B$  in the previous inequalities, using the symmetry property of  $\mathcal{K}_{AB}(t)$ . The main results established below are:

- (i) Formula (64) generalizes Eq. (23) to larger times, giving the time evolution of  $\mathcal{K}_{AB}(t)$  when the gas  $B$  is in the MI regime.
- (ii) Under the same condition, the time-averaged shifted Schmidt number  $\langle \mathcal{K}_{AB} \rangle_t$  is still given by Eq. (24) in the intermediate time regime. In the numerical simulations shown in Fig. 7(a), one indeed observes that  $\langle \mathcal{K}_{AB} \rangle_t$  stays constant over a wide range of time, even at times larger than  $U_A^{-1}$ .
- (iii) Formula (73) generalizes Eq. (31) to larger times, giving the time evolution of  $\mathcal{K}_{AB}(t)$  when the gas  $B$  is in the SF regime.
- (iv) Under the same condition, Eq. (75) shows that the time-averaged shifted Schmidt number  $\langle \mathcal{K}_{AB} \rangle_t$  takes in the intermediate time regime a constant value slightly above the short-time value; we find numerically that  $\langle \mathcal{K}_{AB} \rangle_t$  is constant even at times larger than  $U_A^{-1}$  and  $U_B^{-1}$ , see Fig. 7(b).

The analytical calculations leading to these results are technically more involved than those of the previous sections. Actually, to be able to estimate  $\mathcal{K}_{AB}(t)$  in the intermediate time regime one needs to determine



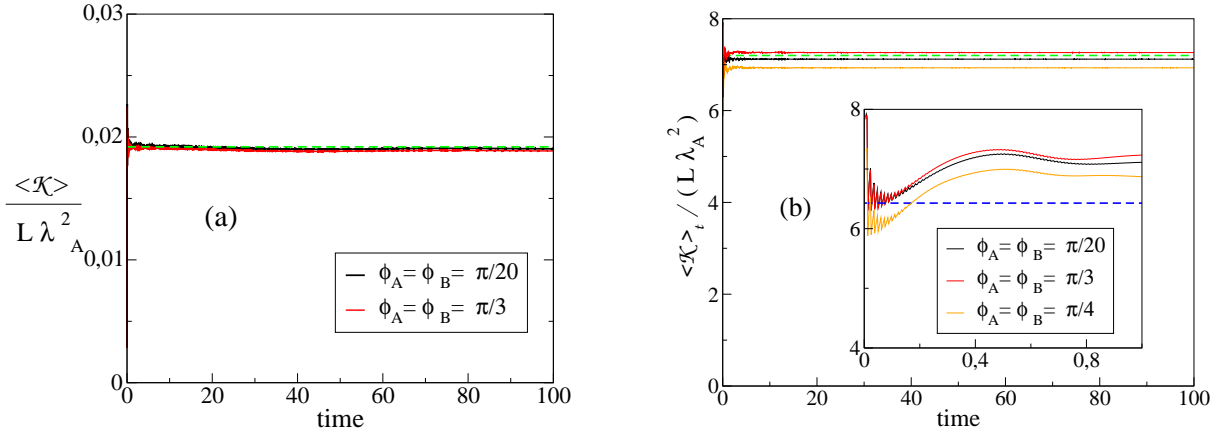


Figure 7: **(a):** Time-averaged Schmidt number per site  $\langle \mathcal{K}_{AB} \rangle_t / L$  divided by  $\lambda_A^2$  as function of time  $t$  (in units of  $U_B^{-1}$ ) for a gas  $B$  in the MI regime up to  $t = 100/U_B$  (from numerical calculations). Parameters:  $L = N_A = N_B = 4$ ,  $V = 100U_B$ ,  $J_B = 0.01U_B$ ,  $U_A = 0.1U_B$ , and  $J_A = 0.001U_B$ ,  $\phi_A = \phi_B = \pi/20$  (black line) and  $\pi/3$  (red line). Horizontal green dashed line: value from Eq. (24). **(b):** Same for a gas  $B$  in the SF regime. Parameters:  $L = N_A = N_B = 4$ ,  $V = 500U_B$ ,  $J_B = 5U_B$ ,  $U_A = 0.1U_B$ ,  $J_A = 0.001U_B$ ,  $\phi_A = \phi_B = \pi/20$  (black line),  $\pi/3$  (red line) and  $\pi/4$  (orange line), with the behaviors at times between 0 and  $U_B^{-1}$  shown in the inset. The horizontal blue and green dashed lines display the values from Eq. (75) in the short and intermediate time regimes, respectively. Note that the phase  $\pi/4$  corresponds to the critical value  $\phi_0/2$  for which Eq. (75) is not valid (see text).

the spectrum and eigenvectors of the Hamiltonian  $\hat{W}_B^{(01)}$  appearing in Eq. (21). This is done in the two limiting cases  $\lambda_B \ll 1$  (gas  $B$  in the MI regime) and  $\lambda_B \gg 1$  (gas  $B$  in the SF regime) in the two next subsections.

### 7.1 Gases $A$ and $B$ in the MI regime

As before, we consider a gas  $A$  initially in the MI regime and inter-species interaction strengths  $V$  much larger than the single species energies, see (3). We assume in this subsection that, in addition, the gas  $B$  is also in the MI regime, i.e.  $\lambda_B \ll 1$ . We determine the shifted Schmidt number in these limits by relying on formula (21), which gives a good approximation of  $\mathcal{K}_{AB}(t)$  at times  $t$  satisfying (43), as shown in Appendix B. Using the spectral decomposition of  $e^{-it\hat{W}_B^{(01)}}$ , this gives

$$\mathcal{K}_{AB}(t) = 4L\alpha_A\lambda_A^2 \left[ 1 - \sum_{\underline{n}, \underline{n}'} \cos(t(w_{\underline{n}} - w_{\underline{n}'})) |\langle \phi_{\underline{n}} | \psi_B \rangle|^2 |\langle \phi_{\underline{n}'} | \psi_B \rangle|^2 \right], \quad (44)$$

where  $|\phi_{\underline{n}}\rangle$  and  $w_{\underline{n}}$  are the eigenstates and eigenenergies of the Hamiltonian  $\hat{W}_B^{(01)}$ . In order to estimate these eigenstates and energies, we diagonalize  $\hat{W}_B^{(01)}$  through a two-fold application of time-independent perturbation theory.

Firstly, we treat the Bose-Hubbard Hamiltonian  $\hat{H}_B$  of the gas  $B$  as a perturbation of  $-V\Delta\hat{n}_{01}^B$ . The latter (unperturbed) Hamiltonian has degenerated eigenvalues  $w_{\Delta}^{(0)} = -V\Delta$  and eigenprojectors

$$\hat{\Pi}_{\Delta} = \sum_{\underline{n}, (\Delta\underline{n})_{01}=\Delta} |\underline{n}\rangle \langle \underline{n}| \quad (45)$$

with  $\Delta \in \{-N_B, \dots, N_B\}$ , where we have set  $(\Delta\underline{n})_{01} \equiv n_1 - n_0$ . Hereafter, we omit the label  $B$  referring to the gas  $B$  to simplify notations. To lowest order in  $U_B/V$ , the eigenstates of  $\hat{W}^{(01)}$  are given by the

eigenstates of the projected Bose-Hubbard Hamiltonian

$$\hat{\Pi}_\Delta \hat{H} \hat{\Pi}_\Delta = \hat{H}^{\text{int}} \hat{\Pi}_\Delta + \hat{\Pi}_\Delta \hat{K} \hat{\Pi}_\Delta \quad (46)$$

and the corresponding eigenvalues are the first-order corrections to the unperturbed energies  $w_\Delta^{(0)}$ . Recall that the kinetic Hamiltonian reads

$$\hat{K} = -J_B \sum_{\langle i,j \rangle} e^{i\phi_{ij}} \hat{b}_j^\dagger \hat{b}_i, \quad (47)$$

where  $\langle i, j \rangle$  refers to nearest neighbor sites  $i, j$  on the ring lattice and  $\phi_{ij} = \pm\phi_B$  if  $j = i \pm 1$ .

For  $\lambda_B \ll 1$ , one may diagonalize the Hamiltonian (46) using once again perturbation theory, now with the intraspecies interaction term  $\hat{H}^{\text{int}} \hat{\Pi}_\Delta$  as the unperturbed part and the projected kinetic Hamiltonian  $\hat{\Pi}_\Delta \hat{K} \hat{\Pi}_\Delta$  as the perturbation. Denote as before by  $E^{(0)}(\underline{n})$  and by  $E_0^{(0)}$  the eigenenergies and GS energy of  $\hat{H}^{\text{int}}$ . For any  $\Delta \in \{-N_B, \dots, N_B\}$  and any energy  $\epsilon$  in the spectrum of  $\hat{H}^{\text{int}} \hat{\Pi}_\Delta$ , let us introduce the set  $\mathcal{S}_{\Delta, \epsilon} = \{\underline{n} \in \mathbb{N}^L; (\Delta \underline{n})_{01} = \Delta, E^{(0)}(\underline{n}) = \epsilon, \sum_j n_j = N_B\}$  and let  $(c_{\underline{m}, \underline{n}})_{\underline{m} \in \mathcal{S}_{\Delta, \epsilon}}$  be the normalized eigenvectors of the matrix  $(\langle \underline{p} | \hat{K} | \underline{m} \rangle)_{\underline{p}, \underline{m} \in \mathcal{S}_{\Delta, \epsilon}}$  with eigenvalues  $E^{(1)}(\underline{n})$ ,  $\underline{n} \in \mathcal{S}_{\Delta, \epsilon}$ . The eigenenergies and eigenstates of  $\hat{W}^{(01)}$  are given by

$$w_{\underline{n}} = -V(\Delta \underline{n})_{01} + E^{(0)}(\underline{n}) + E^{(1)}(\underline{n}) + \mathcal{O}(\lambda_B J_B) + \mathcal{O}\left(\frac{U_B^2}{V}\right) \quad (48)$$

$$|\phi_{\underline{n}}\rangle = |\phi_{\underline{n}}^{(0)}\rangle + \lambda_B |\phi_{\underline{n}}^{(1)}\rangle + \lambda_B^2 |\phi_{\underline{n}}^{(2)}\rangle + \mathcal{O}(\lambda_B^3) + \mathcal{O}\left(\frac{U_B}{V}\right) \quad (49)$$

with  $(\Delta \underline{n})_{01} = \Delta$  and  $E^{(0)}(\underline{n}) = \epsilon$ , where

$$|\phi_{\underline{n}}^{(0)}\rangle = \sum_{\underline{m} \in \mathcal{S}_{\Delta, \epsilon}} c_{\underline{m}, \underline{n}} |\underline{m}\rangle, \quad \lambda_B |\phi_{\underline{n}}^{(1)}\rangle = \sum_{\underline{p}, (\Delta \underline{p})_{01} = \Delta, E^{(0)}(\underline{p}) \neq \epsilon} \frac{|\underline{p}\rangle \langle \underline{p} | \hat{K} | \phi_{\underline{n}}^{(0)} \rangle}{E^{(0)}(\underline{n}) - E^{(0)}(\underline{p})}. \quad (50)$$

In particular, since the GS of  $\hat{H}^{\text{int}}$  is non-degenerated and given by the MI state  $|\psi_{\text{MI}}\rangle = |\underline{\nu}\rangle$ , the set  $\mathcal{S}_{\Delta, \epsilon}$  reduces to a single element  $\underline{\nu}$  when  $\Delta = 0$  and  $\epsilon = E_0^{(0)}$ . Then (compare with (13))

$$|\phi_{\underline{\nu}}^{(0)}\rangle = |\psi_{\text{MI}}\rangle, \quad |\phi_{\underline{\nu}}^{(1)}\rangle = \sqrt{\alpha_B} \sum_{\langle i,j \rangle, \Delta_{01}^{ij}=0} e^{i\phi_{ij}^B} |\underline{\nu} + 1_j - 1_i\rangle, \quad (51)$$

where we have set

$$\Delta_{01}^{ij} = -\Delta_{01}^{ji} = \delta_{1,j} - \delta_{1,i} - \delta_{0,j} + \delta_{0,i} = \begin{cases} 2 & \text{if } i = 0, j = 1 \\ 1 & \text{if } (i = 0, j \notin \{0, 1\}) \text{ or } (i \notin \{0, 1\}, j = 1) \\ 0 & \text{if } i, j \notin \{0, 1\}. \end{cases} \quad (52)$$

Furthermore, the second-order correction is given when  $\Delta = 0$  and  $\epsilon = E_0^{(0)}$  by

$$\begin{aligned} \lambda_B^2 |\phi_{\underline{\nu}}^{(2)}\rangle &= \sum_{\underline{m}, \underline{p} \neq \underline{\nu}, (\Delta \underline{m})_{01} = (\Delta \underline{p})_{01} = 0} \frac{\langle \underline{m} | \hat{K} | \underline{p} \rangle \langle \underline{p} | \hat{K} | \psi_{\text{MI}} \rangle}{(E_0^{(0)} - E^{(0)}(\underline{m}))(E_0^{(0)} - E^{(0)}(\underline{p}))} |\underline{m}\rangle \\ &\quad - \frac{1}{2} \sum_{\underline{m} \neq \underline{\nu}, (\Delta \underline{m})_{01} = 0} \frac{|\langle \underline{m} | \hat{K} | \psi_{\text{MI}} \rangle|^2}{(E_0^{(0)} - E^{(0)}(\underline{m}))^2} |\psi_{\text{MI}}\rangle. \end{aligned} \quad (53)$$

The next step is to calculate the scalar products  $\langle \phi_{\underline{n}} | \psi \rangle$  appearing in (44) up to second order in  $\lambda_B$ . To this end, we combine (49) with the perturbative expansion of the GS  $|\psi\rangle$  of the gas  $B$  analog to (12).

Since  $\hat{K}$  only couples the MI state to Fock states with a single particle-hole excitation and the energy to create such an excitation is equal to  $U_B$ , one has  $\langle \underline{m} | \hat{K} | \psi_{\text{MI}} \rangle \neq 0$  if and only if  $E^{(0)}(\underline{m}) = E_0^{(0)} + U_B$ . Consequently, by (50),

$$\begin{aligned} \lambda_B \langle \phi_{\underline{n}}^{(1)} | \psi_{\text{MI}} \rangle &= \begin{cases} \frac{1}{U_B} \langle \phi_{\underline{n}}^{(0)} | \hat{K} | \psi_{\text{MI}} \rangle & \text{if } (\Delta \underline{n})_{01} = 0 \text{ and } E^{(0)}(\underline{n}) = E_0^{(0)} + U_B \\ 0 & \text{otherwise} \end{cases} \\ &= \begin{cases} -\lambda_B \langle \phi_{\underline{n}}^{(0)} | \psi^{(1)} \rangle & \text{if } (\Delta \underline{n})_{01} = 0 \\ 0 & \text{if } (\Delta \underline{n})_{01} \neq 0, \end{cases} \end{aligned} \quad (54)$$

where we have used (13) (with  $A$  replaced by  $B$ ) in the second equality. Expanding  $|\psi\rangle$  and  $|\phi_{\underline{n}}^{(0)}\rangle$  in powers of  $\lambda_B$  and using  $\langle \phi_{\underline{n}}^{(0)} | \psi_{\text{MI}} \rangle = \delta_{\underline{n}, \underline{\nu}}$ ,  $\langle \phi_{\underline{\nu}}^{(1)} | \psi_{\text{MI}} \rangle = \langle \psi^{(1)} | \psi_{\text{MI}} \rangle = 0$ , and (54), we obtain

$$|\langle \phi_{\underline{n}} | \psi \rangle|^2 = \begin{cases} 1 + 2\lambda_B^2 \text{Re} \{ \langle \phi_{\underline{\nu}}^{(2)} | \psi_{\text{MI}} \rangle + \langle \phi_{\underline{\nu}}^{(1)} | \psi^{(1)} \rangle + \langle \psi_{\text{MI}} | \psi^{(2)} \rangle \} + \mathcal{O}(\lambda_B^3) + \mathcal{O}(\frac{\lambda_B U_B}{V}) & \text{if } \underline{n} = \underline{\nu} \\ \lambda_B^2 |\langle \phi_{\underline{n}}^{(0)} | \psi^{(1)} \rangle|^2 + \mathcal{O}(\lambda_B^3) + \mathcal{O}(\frac{\lambda_B^2 U_B}{V}) & \text{if } \underline{n} \neq \underline{\nu}, (\Delta \underline{n})_{01} \neq 0 \\ \mathcal{O}(\lambda_B^4) + \mathcal{O}(\frac{\lambda_B^3 U_B}{V}) + \mathcal{O}(\frac{\lambda_B^2 U_B^2}{V^2}) & \text{if } \underline{n} \neq \underline{\nu}, (\Delta \underline{n})_{01} = 0. \end{cases} \quad (55)$$

We proceed to evaluate the scalar products appearing in the RHS of (55). One easily shows using (53) that, in analogy with (14),

$$\langle \psi_{\text{MI}} | \phi_{\underline{\nu}}^{(2)} \rangle = -\frac{1}{2} \sum_{\langle i, j \rangle, \Delta_{01}^{ji} = 0} \alpha_B = -\alpha_B (L - 3), \quad (56)$$

where we have taken advantage of (52) in the last equality. Furthermore,  $\langle \phi_{\underline{\nu}}^{(1)} | \psi^{(1)} \rangle$  is given by the same expression multiplied by  $-2$ . Replacing these values into (55), this yields

$$|\langle \phi_{\underline{\nu}} | \psi \rangle|^2 = 1 - 6\lambda_B^2 \alpha_B + \mathcal{O}(\lambda_B^3) + \mathcal{O}(\frac{\lambda_B U_B}{V}). \quad (57)$$

Moreover, one has in view of (13)

$$\langle \phi_{\underline{n}}^{(0)} | \psi^{(1)} \rangle = \begin{cases} \sqrt{\alpha_B} \sum_{\langle i, j \rangle, \Delta_{01}^{ij} = (\Delta \underline{n})_{01}} \overline{c_{\underline{\nu}+1_j-1_i, \underline{n}}} e^{i\phi_{ij}} & \text{if } E^{(0)}(\underline{n}) = E_0^{(0)} + U_B \\ 0 & \text{otherwise.} \end{cases} \quad (58)$$

Plugging the results (48), (55), (57), and (58) into (44) and using the fact that all Fock states with interaction energies  $E^{(0)}(\underline{n}) = E_0^{(0)} + U_B$  have a single particle-hole excitation, that is, there are of the form  $|\underline{n}\rangle = |\underline{\nu} + 1_l - 1_k\rangle$  with  $k \neq l$  not necessarily nearest neighbors, one deduces that

$$\mathcal{K}_{AB}(t) = 8L\alpha_A\alpha_B\lambda_A^2\lambda_B^2 \left[ 6 - \sum_{k \neq l, k \text{ or } l \in \{0,1\}} \mathcal{A}_{kl} \cos \left( t \left( -\Delta_{01}^{kl} V + U_B + E_B^{(1)}(\underline{\nu}_B + 1_l - 1_k) \right) \right) \right] \quad (59)$$

with

$$\mathcal{A}_{kl} \equiv \frac{1}{\alpha_B} |\langle \phi_{\underline{\nu}+1_l-1_k}^{(0)} | \psi^{(1)} \rangle|^2 = \left| \sum_{\langle i, j \rangle, \Delta_{01}^{ij} = \Delta_{01}^{kl}} c_{\underline{\nu}_B+1_j-1_i, \underline{\nu}_B+1_l-1_k} e^{-i\phi_{ij}} \right|^2. \quad (60)$$

The missing error terms inside the square bracket in (59) are of order  $\lambda_B$ ,  $U_B/(\lambda_B V)$ ,  $\lambda_B J_B t$ , and  $U_B^2 t/V$ .

Therefore, by inspection on (52) and (59),  $\mathcal{K}_{AB}(t)$  presents oscillations with frequencies  $2V \pm U_B + \mathcal{O}(J_B)$  and  $V \pm U_B + \mathcal{O}(J_B)$  around the mean value  $\langle \mathcal{K}_{AB} \rangle_t = 48L\alpha_A\alpha_B\lambda_A^2\lambda_B^2$ . In particular, Eq. (24) remains valid when the Schmidt number is averaged over time intervals  $[0, t]$  satisfying

$$V^{-1} \ll t \ll U_A^{-1}, (\lambda_B J_B)^{-1}, VU_B^{-2} \quad (61)$$

(recall that Eq. (24) was shown in Sect. 5.1 to hold in the small time regime  $t \ll U_B^{-1}, U_A^{-1}$  only). Note that for large atom numbers  $N_A, N_B$ , all energy parameters in these inequalities must be multiplied by the corresponding atom number, see the discussion at the end of Sec. 5.2. The averaged Schmidt number  $\langle \mathcal{K}_{AB} \rangle_t$  evaluated numerically is displayed as function of  $t$  in Fig. 7(a). One observes that  $\langle \mathcal{K}_{AB} \rangle_t$  is constant in the time range  $[100V^{-1}, J_B^{-1}]$ . Note that a good agreement with the predicted value from Eq. (24) is obtained even for times  $t$  not satisfying the condition  $t \ll U_A^{-1}$ .

Formula (59) is valid in the intermediate time regime  $t \approx J_B^{-1}$  (with  $J_B \gg U_A, U_B^2/V$ ). We now derive a simpler and more explicit expression for times  $0 \leq t \lesssim U_B^{-1} \ll J_B^{-1}$ . Then the first-order correction  $E_B^{(1)}$  to the eigenenergies (48), which is of order  $J_B$ , can be neglected and one gets

$$\mathcal{K}_{AB}(t) = \langle \mathcal{K}_{AB} \rangle_t - 8L\alpha_A\lambda_A^2\lambda_B^2 \sum_{\Delta=\pm 2, \pm 1} \cos(t(-V\Delta + U_B)) \sum_{\underline{m}, (\Delta \underline{m})_{01}=\Delta, E_B^{(0)}(\underline{m})=E_{0,B}^{(0)}+U_B} |\langle \phi_{\underline{m}}^{(0)} | \psi_B^{(1)} \rangle|^2. \quad (62)$$

But for any eigenenergy  $\epsilon$  of  $\hat{H}_B^{\text{int}}$  one has

$$\sum_{\underline{m} \in \mathcal{S}_{\Delta, \epsilon}} |\langle \phi_{\underline{m}}^{(0)} | \psi_B^{(1)} \rangle|^2 = \sum_{\underline{m} \in \mathcal{S}_{\Delta, \epsilon}} |\langle \underline{m} | \psi_B^{(1)} \rangle|^2. \quad (63)$$

Furthermore, in view of Eq. (13), for any  $\underline{m} \neq \underline{\nu}_B$  it holds  $\langle \underline{m} | \psi_B^{(1)} \rangle = \sqrt{\alpha_B} e^{i\phi_{ij}^B}$  if  $\underline{m} = \underline{\nu}_B + 1_j - 1_i$  with  $i, j$  nearest neighbors and  $\langle \underline{m} | \psi_B^{(1)} \rangle = 0$  otherwise. This yields, using (52) again,

$$\frac{1}{L} \mathcal{K}_{AB}(t) = 8\alpha_A\alpha_B\lambda_A^2\lambda_B^2 \left[ 6 - 4\cos(tV)\cos(tU_B) - 2\cos(2tV)\cos(tU_B) \right] \quad (64)$$

if  $t \ll U_A^{-1}, J_B^{-1}, VU_B^{-2}$ .

Note that this formula agrees with (23) in the short time regime  $t \ll U_B^{-1}, U_A^{-1}$ . The time evolution of  $\mathcal{K}_{AB}(t)$  calculated numerically by exact diagonalization is compared with our analytical result (64) in the inset of Fig. 4(a), showing a good agreement. The presence of the frequency  $U_B$  in Eq. (64), which is the particle-hole excitation energy for the species B, indicates that the entanglement does not only depend on the inter-species interactions but also on the post-quench intra-species interactions.

It is worth observing that the Schmidt number  $\mathcal{K}_{AB}(t)$  being symmetric in  $A$  and  $B$ , the whole calculation above remains valid by exchanging the role of  $A$  and  $B$ . Therefore, the time-averaged Schmidt number is also given by (24) for averages up to time  $t$  satisfying  $V^{-1} \ll t \ll U_B^{-1}, (\lambda_A J_A)^{-1}, VU_A^{-2}$ , instead of (61). Similarly, (64) is correct with  $U_B$  replaced by  $U_A$  when  $t \ll U_B^{-1}, J_A^{-1}, VU_A^{-2}$ . Furthermore, as shown in Appendix B, Eqs. (24) and (64) can be easily extended to Bose-Bose mixtures in arbitrary finite lattices  $\Lambda$  in dimension  $D = 1, 2$ , or  $3$  with periodic boundary conditions, see Eqs. (B.12) and (B.13).

## 7.2 Gases $A$ and $B$ in the MI and SF regimes

Let us now determine the Schmidt number in the intermediate time regime when  $\lambda_B \gg 1$  (gas  $B$  in the SF regime). As in the previous subsection, we rely on the separation of energy scales (3) and determine the spectrum and eigenvectors of  $\hat{W}^{(01)}$  using perturbation theory, the perturbation being the Bose-Hubbard Hamiltonian  $\hat{H}$  of the gas  $B$ . One must diagonalize the projected Hamiltonian

$$\hat{\Pi}_\Delta \hat{H} \Pi_\Delta = \Pi_\Delta \hat{K} \Pi_\Delta + \mathcal{O}(U_B) = \Pi_\Delta \hat{K}' + \mathcal{O}(U_B), \quad (65)$$

where  $\hat{\Pi}_\Delta$  is the projector (45). In the last equality in Eq. (65) we have introduced the kinetic Hamiltonian  $\hat{K}'$  of an open chain  $\Lambda' = \{2, \dots, L-1\}$  with  $(L-2)$  sites,

$$\hat{K}' = -J_B \sum_{j=2}^{L-2} (e^{i\phi_B} \hat{b}_{j+1}^\dagger \hat{b}_j + \text{h.c.}) . \quad (66)$$

The equality  $\Pi_\Delta \hat{K} \Pi_\Delta = \Pi_\Delta \hat{K}'$  follows from the fact that  $\Delta_{01}^{ij} = 0$  if and only if  $i, j \notin \{0, 1\}$ , see (52).

The eigenvectors of  $\Pi_\Delta \hat{K}'$  are given by  $|n_0, n_1\rangle |\phi'_{\sigma,k}\rangle$  with  $n_1 - n_0 = \Delta$  and  $n_0 + n_1 = \sigma$ ,  $|\phi'_{\sigma,k}\rangle$  being the eigenvectors of  $\hat{K}'$  for an atomic gas with  $N_\sigma \equiv N_B - \sigma$  atoms trapped in the chain  $\Lambda'$ , i.e.,  $\hat{K}' |\phi'_{\sigma,k}\rangle = w'_{\sigma,k} |\phi'_{\sigma,k}\rangle$ . Thus the perturbative eigenvalues and eigenvectors of  $\hat{W}^{(01)}$  are

$$w_{n_0, n_1, k} = -V(n_1 - n_0) + w'_{\sigma,k} + \mathcal{O}(U_B) + \mathcal{O}\left(\frac{J_B^2}{V}\right) \quad (67)$$

$$|\phi_{n_0, n_1, k}\rangle = |n_0, n_1\rangle |\phi'_{\sigma,k}\rangle + \mathcal{O}(\lambda_B^{-1}) + \mathcal{O}\left(\frac{J_B}{V}\right) . \quad (68)$$

Using the spectral decomposition  $e^{-it\hat{K}'} = \sum_k e^{-itw'_{\sigma,k}} |\phi'_{\sigma,k}\rangle \langle \phi'_{\sigma,k}|$ , we find

$$\langle \psi | e^{-it\hat{W}^{(01)}} | \psi \rangle = \sum_{n_0, n_1} e^{itV(n_1 - n_0)} \langle \psi | n_0, n_1 \rangle e^{-it\hat{K}'} \langle n_0, n_1 | \psi \rangle \quad (69)$$

up to errors of order  $\lambda_B^{-1}$ ,  $J_B/V$ ,  $U_B t$ , and  $J_B^2 t/V$ . Note that Eq. (69) applies to times satisfying  $t \ll U_B^{-1}$ , in addition to (43), because we have neglected the interaction term  $\Pi_\Delta \hat{H}^{\text{int}}$  in (65); it is, however, justified to use (69) for times  $t \approx J_B^{-1}$ . To simplify we assume that  $-\phi_0/2 \leq \phi_B < \phi_0/2$ , so that the gas  $B$  has zero angular momentum ( $\ell = 0$ ). Replacing  $|\psi\rangle$  by the SF state  $|\psi_{\text{SF}}\rangle$ , a calculation similar to the one performed in Sect. 5.2 leads to

$$\langle \psi | e^{-it\hat{W}^{(01)}} | \psi \rangle = \sum_{\sigma=0}^{N_B} \left( \frac{2 \cos(tV)}{L} \right)^\sigma \frac{N_B!}{\sigma!(N_B - \sigma)!} \left( \frac{L-2}{L} \right)^{N_B - \sigma} R_\sigma(t) \quad (70)$$

with

$$R_\sigma(t) \equiv \langle \psi'_{\text{SF}, \sigma} | e^{-it\hat{K}'} | \psi'_{\text{SF}, \sigma} \rangle . \quad (71)$$

Here,  $|\psi'_{\text{SF}, \sigma}\rangle$  is the SF state of a gas with  $N_\sigma$  atoms and angular momentum  $\ell = 0$  trapped in the ring lattice  $\Lambda'_{\text{ring}} = \{2, \dots, L-1\}$  with  $(L-2)$  sites. Note that the identity (70) does not hold when  $\ell \neq 0$  due to the different values of  $\phi_0$  in the lattices  $\Lambda$  and  $\Lambda'_{\text{ring}}$ .

We now show that in the thermodynamical limit the factor  $R_\sigma(t)$  is equal to  $e^{-itE_{\text{SF}, \sigma}}$ , where  $E_{\text{SF}, \sigma} = -2N_\sigma J_B \cos \phi_B$  is the GS energy of a non-interacting Bose gas with  $N_\sigma$  atoms in the ring lattice  $\Lambda'_{\text{ring}}$ . Actually, let us denote by  $\hat{K}'_{\text{1st q}}$  the first quantization version of (66) and by  $|\varphi_0^{\text{ring}}\rangle$  the GS of a single atom in the ring  $\Lambda'_{\text{ring}}$ . The kinetic Hamiltonian on  $\Lambda'_{\text{ring}}$  differs from  $\hat{K}'_{\text{1st q}}$  by the presence of hopping terms between sites 2 and  $L-1$ , namely by  $\hat{Q} = -J_B(e^{i\phi_B} |2\rangle \langle L-1| + \text{h.c.})$ . We can use second-order perturbation theory to expand  $|\varphi_0^{\text{ring}}\rangle$  in terms of the eigenstates  $|\varphi'_k\rangle$  of  $\hat{K}'_{\text{1st q}}$  and to evaluate  $\langle \varphi_0^{\text{ring}} | e^{-it\hat{K}'_{\text{1st q}}} | \varphi_0^{\text{ring}} \rangle$ . Observing that  $|\langle \varphi'_k | \hat{Q} | \varphi'_0 \rangle|^2$  is typically much smaller than  $L^{-1}$  for large  $L$ 's (the GS and first excited states of the chain  $\Lambda'$  are delocalized on the whole chain), this gives  $\langle \varphi_0^{\text{ring}} | e^{-it\hat{K}'_{\text{1st q}}} | \varphi_0^{\text{ring}} \rangle \simeq e^{-itE'_0} + o(L^{-1})$ , where  $E'_0$  is the GS energy of a single atom in the chain  $\Lambda'$ . Since the SF state is the  $N_\sigma$ -fold tensor product of the single atom state  $|\varphi_0^{\text{ring}}\rangle$  and noting that  $o(L^{-1}) = o(N_\sigma^{-1})$ , one infers that for  $N_\sigma \gg 1$ ,

$$R_\sigma(t) = \langle \varphi_0^{\text{ring}} | e^{-it\hat{K}'_{\text{1st q}}} | \varphi_0^{\text{ring}} \rangle^{N_\sigma} \sim e^{-itN_\sigma E'_0} \sim e^{2itN_\sigma J_B \cos \phi_B} , \quad (72)$$

where we have approximated  $E'_0$  by the GS energy  $E_0^{\text{ring}} = -2J_B \cos \phi_B$  of a single atom in the ring  $\Lambda'_{\text{ring}}$ .

Replacing (70) and (72) into (21), one obtains in the thermodynamical limit  $N_B, L \gg 1$ ,

$$\frac{\mathcal{K}_{AB}(t)}{L} \simeq 4\alpha_A \lambda_A^2 \left( 1 - \exp \left\{ -4\nu_B (1 - \cos(tV) \cos(2tJ_B \cos \phi_B)) \right\} \right). \quad (73)$$

This formula is valid for Peierls phases  $\phi_B$  satisfying  $-\phi_0/2 < \phi_B < \phi_0/2$  and times  $t$  much smaller than  $U_B^{-1}, U_A^{-1}$ , and  $VJ_B^{-2}$ . Notice that one recovers the result of Eq. (31) when  $t \ll J_B^{-1}$ . On the other hand, averaging  $\mathcal{K}_{AB}(t)$  up to times  $t$  with  $J_B^{-1} \ll t \ll U_B^{-1}, U_A^{-1}, VJ_B^{-2}$ , one is led to

$$\frac{\langle \mathcal{K}_{AB} \rangle_t}{L} \simeq 6\alpha_A \lambda_A^2 \beta'_{\nu_B, \infty} \quad , \quad \beta'_{\nu_B, \infty} = \frac{2}{3} \left( 1 - \lim_{k \rightarrow \infty} \int_0^{2\pi k} \frac{ds}{2\pi k} e^{-4\nu_B (1 - \cos(s) \cos(s/k))} \right). \quad (74)$$

This result easily follows by (i) making the change of variables  $s = Vt$  in the integral between 0 and  $t$  of the exponential in (73); (ii) approximating the second cosine by  $\cos(s/k)$  with  $k = E[V/(2J_B \cos \phi_B)]$  (this is justified since  $t \ll VJ_B^{-2}$ ); (iii) using the periodicity of the resulting integrand; (iv) taking  $k = \mathcal{O}(V/J_B) \rightarrow \infty$ .

We may summarize the results of this subsection and those of Sec. 5.2 by the following formula

$$\frac{\langle \mathcal{K}_{AB} \rangle_t}{L} = 6\alpha_A \lambda_A^2 \begin{cases} \beta_{\nu_B, \infty} & \text{if } V^{-1} \ll t \ll J_B^{-1} \\ \beta'_{\nu_B, \infty} & \text{if } J_B^{-1} \ll t \ll U_B^{-1}, U_A^{-1}, VJ_B^{-2}, \end{cases} \quad (75)$$

where  $\beta_{\nu_B, \infty}$  and  $\beta'_{\nu_B, \infty}$  are given by (32) and (74); their numerical values are given in Table 1 for  $\nu_B = 1$  and 2.

We compare in Fig. 5(b) formula (73) with the Schmidt number  $\mathcal{K}_{AB}(t)$  evaluated numerically. One sees that while Eq. (73) describes well the time evolution of  $\mathcal{K}_{AB}(t)$  in the time range  $[0, J_B^{-1}]$ , at later times discrepancies appear; this is likely to be due to contributions of larger frequencies  $1/U_B$  and  $1/U_A$  that have been neglected in (73). In spite of this, one observes in Fig. 7(b) that the averaged Schmidt number  $\langle \mathcal{K}_{AB} \rangle_t$  evaluated numerically for  $L = N_A = N_B = 4$  and  $\lambda_B = 5$  is constant over a wide range of time  $[J_B^{-1}, 100U_B^{-1}]$ , in analogy with what happens when  $B$  is in the MI regime. This indicates that the aforementioned contributions of the frequencies  $1/U_A$  and  $1/U_B$  average out to zero. For Peierls phases  $\phi_A = \phi_B = \pi/20$  and  $\pi/3$ , the constant value agrees reasonably well with the value predicted by Eq. (74) even for times  $t$  not satisfying the conditions  $t \ll U_B^{-1}$  and  $t \ll U_A^{-1}$ , even though a slight dependence on the phase is observed for time  $t$  larger than  $J_B^{-1}$  (in contrast, as seen in the inset, the two curves for the phases  $\pi/20$  and  $\pi/3$  are not distinguishable when  $t \ll J_B^{-1}$ ). On the other hand,  $\langle \mathcal{K}_{AB} \rangle_t$  is smaller for  $\phi_A = \phi_B = \phi_0/2 = \pi/4$ , both in the short time regime  $t \lesssim J_B^{-1}$  and in the intermediate and large time regimes  $J_B^{-1} \lesssim t \leq 100U_B^{-1}$ . As pointed out above, Eqs. (28), (74), and (75) are not valid at this phase value, since the GS of the gas  $B$  is a superposition of SF states with angular momenta  $\ell = 0$  and  $\ell = 1$ . This explains the small disagreement between our numerical and analytical results. We observe on Fig. 7(b) that the values of  $\langle \mathcal{K}_{AB} \rangle_t/L$  for  $\phi_A = \phi_B = \phi_0/2$  are obtained by shifting the curve for  $\phi_A = \phi_B = \pi/20$  or  $\pi/3$  by some time-independent constant of order  $0.5\lambda_A^2$ .

The fact that Eqs. (73) and (74), which have been derived assuming a large ring, describe well the behavior of  $\mathcal{K}_{AB}(t)$  at times  $t \lesssim J_B^{-1}$  and its averaged value at times  $t \gg J_B^{-1}$  for a ring with  $L = 4$  sites is an indication that finite size effects do not play an important role.

## 8 Conclusion

We have studied the dynamics of persistent currents in a binary mixture in the presence of an interaction quench between the species. Assuming that one of the gas components is in the MI regime, we found universal relations between the persistent current of the other species, the visibility before the quench,

and the amount of inter-species entanglement. In particular, for the short time regime, the analytical expressions of the relative variation of the time-averaged current show that it is proportional to the 2-Rényi entropy of entanglement and scales quadratically with the visibility before the quench.

Our results are in principle amenable to experimental realizations. In fact, 1D-ring lattice trapping potentials have been already achieved [68] and artificial gauge fields can be created in various ways [10]. Interaction quench dynamics can be generated using the ability to tune atomic interactions with Feshbach resonances [49, 50, 51]. Finally, time-of-flight techniques for obtaining information on the atomic current are available. In particular, the winding number and current-phase relationship can be extracted from the spiral interference pattern obtained after releasing the trap in the plane of the ring and letting the BEC interfere with another BEC confined initially near its center [62, 63, 64, 12].

Some open problems require further studies. Firstly, even though our numerical simulations indicate a saturation of the Schmidt number at large times, at least after having performed a local time averaging to suppress oscillations with frequency equal to the inter-species interaction strength (see Fig. 7), we can not give a definite answer to the question of a possible convergence of the reduced density matrix of one species to a stationary state. In order to get more insight on the convergence properties of the out-of-equilibrium dynamics, one would need to perform simulations for larger system sizes, which is difficult with our exact diagonalization approach; our analytical approach is also of limited use for this problem because it applies to small or intermediate times.

Secondly, it would be of interest to study the  $B$ -current and entanglement evolutions when the gas  $A$  is in the SF regime, instead of the MI regime. One then expects that this gas could have a stronger effect on the  $B$ -current. Note that for repulsive inter-species interactions and when both species are in the SF regime, it has been shown in [71] that certain initial excitations lead in the gauge free 3-site lattice case to a periodic transfer of angular momentum between the two species. These issues will be investigated in a forthcoming work.

Thirdly, it would be worth adapting our methods to the case of a single impurity atom interacting with a gas of atoms of a different species, taking  $N_A = 1$  and  $N_B \gg 1$  or vice versa in our model. This problem has attracted a lot of interest recently in relation with the polaron physics [44, 45, 46, 47, 48].

**Acknowledgments** D.S. acknowledges support from the Fondecyt project N° 1190134 and the Vicerectoría de Investigación y Desarrollo de la Universidad de Concepción, proyecto VRID 218.013.045-1.OIN, and L. M-M. acknowledges support from the Fondecyt project N° 1190629 and the Vicerectoría de Investigación de la Pontificia Universidad Católica de Chile, proyecto Puente No 03/2019.

## A Visibility of a BEC trapped in a 1D-ring lattice potential

In this appendix we determine the visibility of the interference fringes of a single BEC trapped in a 1D-ring lattice potential in the presence of an artificial gauge field. As mentioned in the main text, the interference pattern is obtained after releasing the potential trap and letting the atomic gas expand freely, thus it is directly related to the momentum distribution

$$S_\phi(q) = \sum_{i,j=0}^{L-1} e^{iq(i-j)} \langle \psi_\phi | \hat{b}_i^\dagger \hat{b}_j | \psi_\phi \rangle, \quad (\text{A.1})$$

where  $|\psi_\phi\rangle$  is the ground state (GS) of the Bose-Hubbard Hamiltonian  $\hat{H}_\phi$  of a single species (Eq. (1) in the main text),  $\phi$  is the Peierls phase,  $\hat{b}_i^\dagger$  and  $\hat{b}_j$  are the creation and annihilation operators of a bosonic

atom at sites  $i$  and  $j$ , and  $L$  is the number of lattice sites. The visibility is defined as

$$\mathcal{V}_\phi = \frac{S_{\max} - S_{\min}}{S_{\max} + S_{\min}}, \quad (\text{A.2})$$

$S_{\max}$  and  $S_{\min}$  being the maximum and minimum of  $S_\phi(q)$ . By gauge invariance,  $\mathcal{V}_\phi$  is periodic in  $\phi$  with period  $\phi_0 = 2\pi/L$ . Actually, the Hamiltonians  $\hat{H}_{\phi+\phi_0}$  and  $\hat{H}_\phi$  and their GSs are related by a gauge transformation, e.g.  $|\psi_{\phi+\phi_0}\rangle = e^{i\phi_0\hat{X}}|\psi_\phi\rangle$  with  $\hat{X} = \sum_j j\hat{b}_j^\dagger\hat{b}_j$ , implying that  $S_{\phi+\phi_0}(q) = S_\phi(q - \phi_0)$ .

We determine analytically the momentum distribution and visibility when the Bose gas is in the Mott-insulator (MI) regime, i.e., for small energy ratio  $\lambda = J/U$ . We rely on standard perturbation theory, the perturbation being the kinetic term

$$\hat{K}_\phi = -J \sum_{j=0}^{L-1} (e^{i\phi}\hat{b}_{j+1}^\dagger\hat{b}_j + \text{h.c.}). \quad (\text{A.3})$$

As in the main text, the Fock states diagonalizing  $\hat{H}^{\text{int}} = \hat{H}_\phi - \hat{K}_\phi$  are denoted by  $|\underline{n}\rangle = |n_0, \dots, n_{L-1}\rangle$ ,  $E^{(0)}(\underline{n})$  are the corresponding eigenenergies, the filling factor  $\nu = N/L$  is assumed to be an integer, and  $|\psi_{\text{MI}}\rangle = |\underline{\nu}\rangle = |\nu, \dots, \nu\rangle$  is the MI state (GS of  $\hat{H}^{\text{int}}$  with energy  $E_0^{(0)} = E(\underline{\nu})$ ). For small  $\lambda$ , the GS of the BEC reads

$$|\psi_\phi\rangle = |\psi_{\text{MI}}\rangle + \lambda|\psi_\phi^{(1)}\rangle + \lambda^2|\psi_\phi^{(2)}\rangle + \mathcal{O}(\lambda^3) \quad (\text{A.4})$$

with the first and second-order corrections

$$\lambda|\psi_\phi^{(1)}\rangle = -\frac{1}{U}\hat{K}_\phi|\psi_{\text{MI}}\rangle = \lambda \sum_{j=0}^{L-1} (e^{i\phi}\hat{b}_{j+1}^\dagger\hat{b}_j + \text{h.c.})|\psi_{\text{MI}}\rangle \quad (\text{A.5})$$

$$\lambda^2|\psi_\phi^{(2)}\rangle = \sum_{\underline{m}, \underline{p} \neq \underline{\nu}} \frac{\langle \underline{m}|\hat{K}_\phi|\underline{p}\rangle \langle \underline{p}|\hat{K}_\phi|\psi_{\text{MI}}\rangle}{(E_0^{(0)} - E^{(0)}(\underline{m}))(E_0^{(0)} - E^{(0)}(\underline{p}))} |\underline{m}\rangle - \frac{1}{2} \sum_{\underline{m} \neq \underline{\nu}} \frac{|\langle \underline{m}|\hat{K}_\phi|\psi_{\text{MI}}\rangle|^2}{(E_0^{(0)} - E^{(0)}(\underline{m}))^2} |\psi_{\text{MI}}\rangle. \quad (\text{A.6})$$

Here, we have used  $\langle \psi_{\text{MI}}|\hat{K}_\phi|\psi_{\text{MI}}\rangle = 0$  and the fact that the energy to create a particle-hole excitation  $\propto \hat{b}_i^\dagger\hat{b}_j|\psi_{\text{MI}}\rangle$  is equal to

$$E^{(0)}(\underline{\nu} + 1_i - 1_j) - E_0^{(0)} = U, \quad i \neq j, \quad (\text{A.7})$$

where  $1_j = (0, \dots, 1, 0, \dots, 0)$  is the vector having a single nonzero component equal to unity at site  $j$ . Noting that  $\langle \underline{m}|\hat{K}_\phi|\psi_{\text{MI}}\rangle = 0$  if  $E^{(0)}(\underline{m}) \neq E_0^{(0)} + U$ , one deduces from (A.6) that

$$\lambda^2\langle \psi_{\text{MI}}|\psi_\phi^{(2)}\rangle = -\frac{1}{2U^2}\langle \psi_{\text{MI}}|\hat{K}_\phi^2|\psi_{\text{MI}}\rangle = -\frac{\lambda^2}{2}\|\psi_\phi^{(1)}\|^2 = -\nu(\nu+1)\lambda^2L. \quad (\text{A.8})$$

Substituting (A.4) into (A.1), the momentum distribution reads

$$\begin{aligned} S_\phi(q) &= \sum_{i,j=0}^{L-1} e^{iq(i-j)} \langle \psi_{\text{MI}}|\hat{b}_i^\dagger\hat{b}_j|\psi_{\text{MI}}\rangle + 2\lambda \text{Re} \left\{ \sum_{i,j=0}^{L-1} e^{iq(i-j)} \langle \psi_{\text{MI}}|\hat{b}_i^\dagger\hat{b}_j|\psi_\phi^{(1)}\rangle \right\} \\ &+ 2\lambda^2 \text{Re} \left\{ \sum_{i,j=0}^{L-1} e^{iq(i-j)} \langle \psi_{\text{MI}}|\hat{b}_i^\dagger\hat{b}_j|\psi_\phi^{(2)}\rangle \right\} + \lambda^2 \sum_{i,j=0}^{L-1} e^{iq(i-j)} \langle \psi_\phi^{(1)}|\hat{b}_i^\dagger\hat{b}_j|\psi_\phi^{(1)}\rangle + \mathcal{O}(\lambda^3). \end{aligned} \quad (\text{A.9})$$



A simple calculation yields

$$\begin{aligned}
\langle \psi_{\text{MI}} | \hat{b}_i^\dagger \hat{b}_j | \psi_{\text{MI}} \rangle &= \nu \delta_{ij} \\
\langle \psi_{\text{MI}} | \hat{b}_i^\dagger \hat{b}_j | \psi_\phi^{(1)} \rangle &= \nu(\nu+1)(1-\delta_{i,j}) \sum_{l=0}^{L-1} \left( e^{i\phi} \delta_{i,l} \delta_{j,l+1} + e^{-i\phi} \delta_{i,l+1} \delta_{j,l} \right) \\
\langle \psi_{\text{MI}} | \hat{b}_i^\dagger \hat{b}_j | \psi_\phi^{(2)} \rangle &= \nu(\nu+1) \left[ (1-\delta_{i,j}) \sum_{l=0}^{L-1} \left( (\nu+1) e^{2i\phi} \delta_{i,l} \delta_{j,l+2} + \nu e^{2i\phi} \delta_{i,l-1} \delta_{j,l+1} \right. \right. \\
&\quad \left. \left. + (\nu+1) e^{-2i\phi} \delta_{i,l+1} \delta_{j,l-1} + \nu e^{-2i\phi} \delta_{i,l+2} \delta_{j,l} \right) - \nu L \delta_{i,j} \right] \\
\langle \psi_\phi^{(1)} | \hat{b}_i^\dagger \hat{b}_j | \psi_\phi^{(1)} \rangle &= \langle \psi_{\text{MI}} | \hat{b}_i^\dagger \hat{b}_j | \psi_\phi^{(2)} \rangle + 3\nu^2(\nu+1)L\delta_{i,j},
\end{aligned} \tag{A.10}$$

where, according to the periodic boundary conditions,  $\delta_{j,L}$  must be identified with  $\delta_{j,0}$ , etc... Note that the expressions (A.10) for  $i = j$  immediately follow from  $\hat{b}_i^\dagger \hat{b}_i | \psi_{\text{MI}} \rangle = \nu | \psi_{\text{MI}} \rangle$ ,  $\langle \psi_{\text{MI}} | \psi_\phi^{(1)} \rangle = 0$ , and (A.8). Plugging (A.10) into (A.9), one finds

$$\begin{aligned}
S_\phi(q) &= L\nu \left\{ 1 + 4(\nu+1)\lambda \left[ \left(1 - \frac{1}{L}\right) \cos(q-\phi) + \frac{1}{L} \cos(q(L-1)+\phi) \right] \right. \\
&\quad \left. + 6(\nu+1)(2\nu+1)\lambda^2 \left[ \left(1 - \frac{2}{L}\right) \cos(2(q-\phi)) + \frac{2}{L} \cos(q(L-2)+2\phi) \right] + \mathcal{O}(\lambda^3) \right\}.
\end{aligned} \tag{A.11}$$

One easily checks that this expression fulfills  $S_{\phi+\phi_0}(q) = S_\phi(q-\phi_0)$  (gauge invariance) and  $S_{-\phi}(q) = S_\phi(-q)$ . As a consequence, the visibility (A.2) satisfies  $\mathcal{V}_{\phi_0 \mp \phi} = \mathcal{V}_\phi$  and it is enough to let  $\phi$  varies between 0 and  $\phi_0/2 = \pi/L$ .

A non-perturbative expression of  $S(q)$  has been determined in Refs. [65, 67] for infinite lattices in the absence of gauge field. Expanding the result of the first reference for small  $\lambda$ 's, one recovers Eq.(A.11) in the special case  $\phi = 0$  and for an infinite ring ( $L \rightarrow \infty$ ), up to an irrelevant constant term. However, as stressed in the main text, we are interested in this article in finite rings with a non-zero gauge field.

We now determine the extrema of  $S_\phi(q)$ . We assume  $L \geq 3$  and  $\lambda \geq 0$ . One has

$$\begin{aligned}
\frac{\partial S_\phi}{\partial q} &= -4\lambda L\nu(\nu+1) \left\{ \left(1 - \frac{1}{L}\right) \left[ \sin(q-\phi) + \sin(q(L-1)+\phi) \right] \right. \\
&\quad \left. + 3\lambda(2\nu+1) \left(1 - \frac{2}{L}\right) \left[ \sin(2(q-\phi)) + \sin(q(L-2)+2\phi) \right] + \mathcal{O}(\lambda^3) \right\}.
\end{aligned} \tag{A.12}$$

We first obtain the extrema of  $S_\phi$  to lowest order in  $\lambda$ . Neglecting the terms of order  $\lambda^2$ ,  $\partial S_\phi / \partial q$  vanishes when  $q - \phi = -(q(L-1) + \phi) + 2m\pi$  or  $q - \phi = q(L-1) + \phi - (2m+1)\pi$ , i.e.,

$$q = q_m = \frac{2m\pi}{L} \quad \text{or} \quad q = q'_m = \frac{(2m+1)\pi - 2\phi}{L-2} \tag{A.13}$$

with  $m$  an arbitrary integer. At these extremal points,  $S_\phi(q)$  takes the values

$$\begin{aligned}
S_\phi(q_m) &= L\nu \left\{ 1 + 4(\nu+1)\lambda \cos(q_m - \phi) + \mathcal{O}(\lambda^2) \right\} \\
S_\phi(q'_m) &= L\nu \left\{ 1 + 4(\nu+1) \left(1 - \frac{2}{L}\right) \lambda \cos(q'_m - \phi) + \mathcal{O}(\lambda^2) \right\}.
\end{aligned} \tag{A.14}$$

To determine which of the extremal points  $q_m, q'_m$  corresponds to the global maximum (minimum), we are left with the task of maximizing (minimizing)  $C_m(\phi) = \cos(q_m - \phi)$  and  $C'_m(\phi) = \cos(q'_m - \phi)$  over all  $m \in \{0, \dots, L-1\}$  and  $m \in \{0, \dots, L-3\}$ , respectively.

Under the assumption  $0 \leq \phi \leq \pi/L$ , one has  $\max_m \{C_m(\phi)\} = C_0(\phi) = \cos \phi$ . Furthermore, it follows from the bound  $1 - 2/L < \cos(\pi/L)$  that for any  $m$ ,

$$-\cos\left(\frac{\pi}{L}\right) < \left(1 - \frac{2}{L}\right)C'_m(\phi) < \cos\left(\frac{\pi}{L}\right) \leq \cos \phi. \quad (\text{A.15})$$

Thus, to lowest order in  $\lambda$ , the maximum of  $S_\phi(q)$  is reached for  $q = q_0 = 0$  modulo  $2\pi$ . Since the term of order  $\lambda^2$  in the derivative in Eq.(A.12) also vanishes for  $q = q_0$ , the exact momenta at which  $S_\phi(q)$  reaches its maximum differ from  $q_0, q_0 \pm 2\pi, \dots$  by at most  $\mathcal{O}(\lambda^2)$ . The value of the maximum is

$$S_{\max} = L\nu \left\{ 1 + 4(\nu + 1)\lambda \cos \phi + 6(\nu + 1)(2\nu + 1)\lambda^2 \cos(2\phi) + \mathcal{O}(\lambda^3) \right\}. \quad (\text{A.16})$$

Similarly,  $\min_m \{C_m(\phi)\} = C_{L/2}(\phi) = -\cos \phi$  if the number of sites  $L$  is even and  $\min_m \{C_m(\phi)\} = C_{(L+1)/2}(\phi) = -\cos(\pi/L - \phi)$  if  $L$  is odd. By (A.15), the minimum of  $S_\phi(q)$  is, to lowest order in  $\lambda$ , reached for  $q = q_{L/2} = \pi$  modulo  $2\pi$  in the first case and for  $q = q_{(L+1)/2} = \pi + \pi/L$  modulo  $2\pi$  in the last case. Again, the term of order  $\lambda^2$  in the derivative in (A.12) vanishes at these momenta, thus these formulas give the locations of the momenta minimizing  $S_\phi(q)$  up to corrections of order  $\mathcal{O}(\lambda^2)$ . The value of the minimum is

$$S_{\min} = \begin{cases} L\nu \left\{ 1 - 4(\nu + 1)\lambda \cos \phi + 6(\nu + 1)(2\nu + 1)\lambda^2 \cos(2\phi) + \mathcal{O}(\lambda^3) \right\} & \text{if } L \text{ is even} \\ L\nu \left\{ 1 - 4(\nu + 1)\lambda \cos\left(\frac{\pi}{L} - \phi\right) + 6(\nu + 1)(2\nu + 1)\lambda^2 \cos\left(\frac{2\pi}{L} - 2\phi\right) + \mathcal{O}(\lambda^3) \right\} & \text{if } L \text{ is odd.} \end{cases} \quad (\text{A.17})$$

We note that when  $\phi = \pi/L$  (respectively  $\phi = 0$  and  $L$  is odd),  $S_\phi(q)$  reaches its maximum (minimum) at two phase points in the interval  $[0, 2\pi]$ , namely at  $q_0 = 0$  and  $q_1 = 2\pi/L$  (respectively at  $q_{(L+1)/2} = \pi + \pi/L$  and  $q_{(L-1)/2} = \pi - \pi/L$ ), up to errors  $\mathcal{O}(\lambda^2)$ .

Even though we are considering a gas in the MI regime, it is convenient to introduce the angular momentum of the superfluid (SF) state,  $\ell = E[\phi/\phi_0 + 1/2]$ , where  $E$  denotes the integer part, and similarly let  $k = E[\phi/\phi_0]$ . The introduction of the integers  $\ell$  and  $k$  helps to write the result in a concise form for arbitrary phases  $\phi \in \mathbb{R}$ , taking into account the periodicity and symmetry properties  $\mathcal{V}_{\pm\phi+\phi_0} = \mathcal{V}_\phi$ . We conclude from (A.16) and (A.17) that if  $L$  is even,  $L \geq 4$ , the visibility is given by

$$\mathcal{V}_\phi = 4(\nu + 1)\lambda \cos(\phi - \ell\phi_0) + \mathcal{O}(\lambda^3) \quad , \quad L \text{ even.} \quad (\text{A.18})$$

If  $L$  is odd,  $L \geq 3$ , it is given by

$$\mathcal{V}_\phi = 2(\nu + 1)\lambda \left[ \cos\left(\frac{\phi_0}{2} - \phi + k\phi_0\right) + \cos(\phi - \ell\phi_0) \right] \times \\ \left\{ 1 - (4\nu + 1)\lambda \left[ \cos\left(\frac{\phi_0}{2} - \phi + k\phi_0\right) - \cos(\phi - \ell\phi_0) \right] \right\} + \mathcal{O}(\lambda^3) \quad , \quad L \text{ odd.} \quad (\text{A.19})$$

Note that in the absence of gauge field, the visibility of ring lattices with even numbers of sites  $L$  coincides with the visibility of an infinite chain,  $\mathcal{V}_{\phi=0} = 4(\nu + 1)\lambda + \mathcal{O}(\lambda^3)$ . The latter has been determined in Ref. [65]. In contrast, for finite odd numbers of sites  $\mathcal{V}_{\phi=0} = 2(\nu + 1)(1 + \cos(\pi/L))\lambda + \mathcal{O}(\lambda^2)$  differs from the aforementioned gauge-free result of Ref. [65], which holds in the large  $L$  limit only.

It is easy to show from Eqs. (A.18) and (A.19) that  $\mathcal{V}_\phi$  is minimum at half-integer values of  $\phi_0$ . If  $L$  is even, this follows from the fact that  $\cos(\phi - \ell\phi_0)$  is minimum at such phase values. If  $L$  is odd, the first-order contribution to the visibility in (A.19) is minimum for  $\phi = m\phi_0$  and  $\phi = (m + 1/2)\phi_0$ , with  $m \in \mathbb{Z}$ . By comparing the second-order corrections, one sees that  $\mathcal{V}_\phi$  reaches its minimum for the latter phase point.

The visibility is displayed as function of  $\phi$  in Fig. 8 (lower panels) for ring lattices with  $L = 4$  and 5 sites and  $\lambda = 0.01$ . The values obtained from Eqs. (A.18)-(A.19) agree well with those obtained by locating

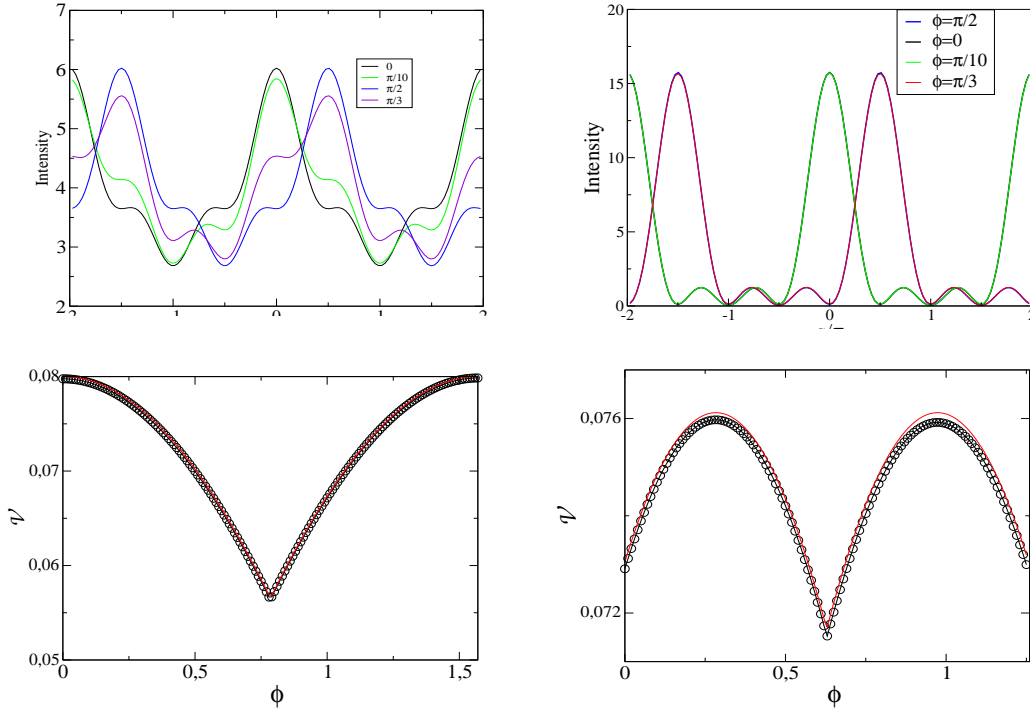


Figure 8: **Upper panels:** momentum distribution  $S_\phi(q)$  (in arbitrary units) as function of  $q$  for a single BEC in the MI regime (left panel,  $\lambda = J/U = 0.05$ ) and in the SF regime (right panel,  $\lambda = 1$ ), from numerical calculations;  $N = 4$  atoms are trapped in a 1D-ring lattice potential with  $L = 4$  sites and Peierls phases  $\phi = 0, \pi/10, \pi/3$ , and  $\pi/2$ . **Lower panels:** visibility of a Bose gas in the MI regime as function of the Peierls phase for  $N = L = 4$  (left panel) and  $N = L = 5$  (right panel), with  $\lambda = J/U = 0.01$ . The black circles correspond to numerical calculations and the red plain curves to Eqs. (A.18) and (A.19).

numerically the extrema of the momentum distribution. The latter is obtained numerically via an exact diagonalization of the Bose-Hubbard Hamiltonian. We have also calculated numerically the momentum distribution and visibility for a gas in the SF regime ( $\lambda = 1$ ) and in the transition regime ( $\lambda \simeq 0.2$ ). The plots of the visibility in the transition regime are shown in Fig. 2 in the main text. The plots of the momentum distribution in the SF and MI regimes are displayed in Fig. 8 (upper panels). We find from our numerical results that the locations of the global extrema of  $S_\phi(q)$  are the same in both regimes. For instance, it is seen in Fig. 8 that  $S_\phi(q)$  reaches its maximum at  $q = \ell\phi_0$  modulo  $2\pi$  in both regimes.

## B Schmidt number as an expectation of a local time-evolution operator

In this appendix we derive formula (21) for the shifted Schmidt number  $\mathcal{K}_{AB}(t)$  quantifying the entanglement between the two gases after interspecies interactions have been switched on.

Our analysis applies here to trapping potentials forming an arbitrary finite lattice  $\Lambda$  with  $L$  sites in dimension  $D = 1, 2$ , or  $3$ , with periodic boundary conditions. We denote by  $z$  the number of nearest neighbors of a given site  $i \in \Lambda$ . For instance,  $z = 2$  for a 1D ring lattice and  $z = 4$  for a 2D square lattice. As we will show below, the Schmidt number turns out to depend on the geometry of the lattice through  $L$  and  $z$  only. The kinetic part  $\hat{K}_B$  of the Bose-Hubbard Hamiltonian of the gas  $B$  is given by Eq. (47) in the main text, where the sum runs over all pairs of nearest neighbor sites  $i, j \in \Lambda$  and the phases  $\phi_{ij} \in \{\phi_B, -\phi_B\}$  are translation-invariant, invariant under rotation over the origin, and satisfy  $\phi_{ji} = -\phi_{ij}$  for any neighboring sites  $i$  and  $j$ , in order to insure that  $\hat{K}_B$  be self-adjoint. A similar expression holds

for the kinetic Hamiltonian  $\hat{K}_A$  of the gas  $A$ .

The wavefunction of the Bose mixture at time  $t$  is  $|\psi_{AB}(t)\rangle = e^{-it\hat{H}_{AB}}|\psi_A\rangle \otimes |\psi_B\rangle$ , where  $\hat{H}_{AB}$  is the Hamiltonian after interactions have been turned on [see Eq. (2) in the main text] and  $|\psi_A\rangle$  and  $|\psi_B\rangle$  are the GSs of the gases  $A$  and  $B$ . We assume that the gas  $A$  is in the MI regime ( $\lambda_A \ll 1$ ), so that  $|\psi_A\rangle$  has the form given in (A.4). Expanding in powers of  $\lambda_A$ , the reduced density matrix of the gas  $A$  reads

$$\hat{\rho}_A(t) = \text{tr}_B[|\psi_{AB}(t)\rangle\langle\psi_{AB}(t)|] = \hat{\rho}_A^{(0)}(t) + \lambda_A \hat{\rho}_A^{(1)}(t) + \lambda_A^2 \hat{\rho}_A^{(2)}(t) + \mathcal{O}(\lambda_A^3) \quad (\text{B.1})$$

with

$$\begin{aligned} \hat{\rho}_A^{(0)}(t) &= \text{tr}_B [e^{-it\hat{H}_{AB}}|\psi_{\text{MI}}\rangle\langle\psi_{\text{MI}}| \otimes |\psi_B\rangle\langle\psi_B| e^{it\hat{H}_{AB}}] \\ \hat{\rho}_A^{(1)}(t) &= \text{tr}_B [e^{-it\hat{H}_{AB}}(|\psi_A^{(1)}\rangle\langle\psi_{\text{MI}}| + |\psi_{\text{MI}}\rangle\langle\psi_A^{(1)}|) \otimes |\psi_B\rangle\langle\psi_B| e^{it\hat{H}_{AB}}] \\ \hat{\rho}_A^{(2)}(t) &= \text{tr}_B [e^{-it\hat{H}_{AB}}(|\psi_A^{(2)}\rangle\langle\psi_{\text{MI}}| + |\psi_{\text{MI}}\rangle\langle\psi_A^{(2)}| + |\psi_A^{(1)}\rangle\langle\psi_A^{(1)}|) \otimes |\psi_B\rangle\langle\psi_B| e^{it\hat{H}_{AB}}] . \end{aligned} \quad (\text{B.2})$$

For times  $t$  satisfying  $t \ll U_A^{-1}$ , the kinetic Hamiltonian  $\hat{K}_A$  of the gas  $A$  can be dropped out, so that

$$\hat{H}_{AB} \simeq \hat{H}_A^{\text{int}} + \underbrace{\hat{H}_B^{\text{int}} + \hat{K}_B + \hat{H}_{AB}^{\text{int}}}_{=\hat{H}_B} , \quad \hat{H}_{AB}^{\text{int}} = -V \hat{n}_A \cdot \hat{n}_B = -V \sum_{j \in \Lambda} \hat{n}_j^A \hat{n}_j^B \quad (\text{B.3})$$

(for simplicity we do not write the identity operators explicitly, e.g.,  $\hat{H}_A^{\text{int}}$  stands for  $\hat{H}_A^{\text{int}} \otimes \hat{\mathbf{1}}_B$ ). Making this approximation in (B.2) and using  $\hat{H}_A^{\text{int}}|\psi_{\text{MI}}\rangle = E_{0,A}^{(0)}|\psi_{\text{MI}}\rangle$  and  $\hat{H}_{AB}^{\text{int}}|\psi_{\text{MI}}\rangle = -V\nu_A N_B |\psi_{\text{MI}}\rangle$ , one easily finds that  $\hat{\rho}_A^{(0)}(t)$  is independent of time and given by

$$\hat{\rho}_A^{(0)}(t) = |\psi_{\text{MI}}\rangle\langle\psi_{\text{MI}}| . \quad (\text{B.4})$$

Consequently, plugging (B.1) and (B.4) into Eq. (20) in the main text,

$$(\mathcal{K}_{AB}(t) + 1)^{-1} = 1 + 2\lambda_A \langle\psi_{\text{MI}}|\hat{\rho}_A^{(1)}(t)|\psi_{\text{MI}}\rangle + 2\lambda_A^2 \langle\psi_{\text{MI}}|\hat{\rho}_A^{(2)}(t)|\psi_{\text{MI}}\rangle + \lambda_A^2 \text{tr} [\hat{\rho}_A^{(1)}(t)^2] + \mathcal{O}(\lambda_A^3) . \quad (\text{B.5})$$

The linear term in  $\lambda_A$  vanishes. In fact,  $\langle\psi_{\text{MI}}|\hat{\rho}_A^{(1)}(t)|\psi_{\text{MI}}\rangle = 2\text{Re} \langle\psi_{\text{MI}}|\psi_A^{(1)}\rangle$  by (B.2) and (B.3), and  $\langle\psi_{\text{MI}}|\psi_A^{(1)}\rangle = 0$ , see (A.5). Generalizing (A.8) to the case of a general lattice  $\Lambda$ , one has

$$\lambda_A^2 \langle\psi_{\text{MI}}|\hat{\rho}_A^{(2)}(t)|\psi_{\text{MI}}\rangle = 2\lambda_A^2 \text{Re} \langle\psi_{\text{MI}}|\psi_A^{(2)}\rangle = -\lambda_A^2 \alpha_A L z \quad (\text{B.6})$$

with  $\alpha_A = \nu_A(\nu_A + 1)$ .

Therefore, the only time-dependent contribution to  $\mathcal{K}_{AB}(t)$  is due to the trace of  $\hat{\rho}_A^{(1)}(t)^2$  in (B.5), which can be estimated as follows. Let us set  $\hat{A}^{(1)} = |\psi_A^{(1)}\rangle\langle\psi_{\text{MI}}| + |\psi_{\text{MI}}\rangle\langle\psi_A^{(1)}|$ . Since  $|\psi_A^{(1)}\rangle = -J_A^{-1} \hat{K}_A |\psi_{\text{MI}}\rangle$ , see A.5, it holds

$$|\langle\mathbf{n}_A|\hat{A}^{(1)}|\mathbf{m}_A\rangle|^2 = \alpha_A \sum_{\langle i,j \rangle} \delta_{\mathbf{n}_A, \mathbf{z}_A + 1_j - 1_i} \delta_{\mathbf{m}_A, \mathbf{z}_A} + (\mathbf{n}_A \leftrightarrow \mathbf{m}_A) \quad (\text{B.7})$$

with  $|\mathbf{z}_A + 1_j - 1_i\rangle$  the Fock state differing from  $|\psi_{\text{MI}}\rangle$  by the presence of an extra particle at site  $j$  and a hole at site  $i$ . By evaluating the trace in the Fock basis  $\{|\mathbf{n}_A\rangle\}$  diagonalizing both  $\hat{n}^A$  and  $\hat{H}_A^{\text{int}}$ , one gets from (B.2) and (B.3)

$$\begin{aligned} \text{tr}_A [\hat{\rho}_A^{(1)}(t)^2] &= \sum_{\mathbf{n}_A, \mathbf{m}_A} |\langle\mathbf{n}_A|\hat{\rho}_A^{(1)}(t)|\mathbf{m}_A\rangle|^2 \\ &= \sum_{\mathbf{n}_A, \mathbf{m}_A} |\langle\mathbf{n}_A|\hat{A}^{(1)}|\mathbf{m}_A\rangle\langle\psi_B|e^{it(\hat{H}_B - V\mathbf{m}_A \cdot \hat{n}_B)}e^{-it(\hat{H}_B - V\mathbf{n}_A \cdot \hat{n}_B)}|\psi_B\rangle|^2 \\ &= 2\alpha_A \sum_{\langle i,j \rangle} |\langle\psi_B|e^{it(\hat{H}_B - V\nu_A \hat{N}_B)}e^{-it(\hat{H}_B - V\nu_A \hat{N}_B - V(\hat{n}_j^B - \hat{n}_i^B))}|\psi_B\rangle|^2 . \end{aligned} \quad (\text{B.8})$$

Thanks to the commutation of the Bose-Hubbard Hamiltonian  $\hat{H}_B$  with the total number operator  $\hat{N}_B$  of the  $B$ -atoms and since  $|\psi_B\rangle$  is an eigenstate of  $\hat{H}_B$ , it holds

$$|\langle\psi_B|e^{it(\hat{H}_B-V\nu_A\hat{N}_B)}e^{-it(\hat{H}_B-V\nu_A\hat{N}_B-V(\hat{n}_j^B-\hat{n}_i^B))}|\psi_B\rangle| = |\langle\psi_B|e^{-it(\hat{H}_B-V(\hat{n}_j^B-\hat{n}_i^B))}|\psi_B\rangle|. \quad (\text{B.9})$$

Now, it follows from the translation-invariance of  $\hat{H}_B$  and its invariance under rotations around the origin that

$$\langle\psi_B|e^{-it(\hat{H}_B-V(\hat{n}_j^B-\hat{n}_i^B))}|\psi_B\rangle = \langle\psi_B|e^{-it(\hat{H}_B-V(\hat{n}_1^B-\hat{n}_0^B))}|\psi_B\rangle \quad \text{if } i, j \text{ are nearest neighbors,} \quad (\text{B.10})$$

where 1 denotes an arbitrary nearest neighbor site to the origin 0. Collecting the above results, one finds

$$\mathcal{K}_{AB}(t) = 2Lz\alpha_A\lambda_A^2\left(1 - |\langle\psi_B|e^{-it(\hat{H}_B-V(\hat{n}_1^B-\hat{n}_0^B))}|\psi_B\rangle|^2\right) + \mathcal{O}(\lambda_A^3). \quad (\text{B.11})$$

For a 1D-ring lattice, this formula reduces to Eq. (21) in the main text.

Recall that Eq. (B.11) has been obtained by neglecting the kinetic Hamiltonian  $\hat{K}_A$  of the gas  $A$  in the dynamics following the interaction quench. Since  $\mathcal{K}_{AB}(t)$  is of order  $\lambda_A^2$ , this is justified *a posteriori* provided that the product  $J_At$  is much smaller than  $\lambda_A$ . In fact, by including in our calculations the corrections due to  $\hat{K}_A$  estimated from time-dependent perturbation theory, one finds that such corrections are of order  $(J_At)^2$  and  $\lambda_A(J_At)$  (all terms proportional to  $J_A$  vanish due to  $\langle\psi_{\text{MI}}|\hat{K}_A|\psi_{\text{MI}}\rangle = 0$ ). Hence the expression in the RHS of (B.11) approximates well  $\mathcal{K}_{AB}(t)$  for times satisfying  $t \ll U_A^{-1}$ , as one may suspect from the fact that neither  $J_A$  nor  $U_A$  appear in this expression.

Let us note that it is straightforward to extend the arguments of Sect. 7.1 to the case of an arbitrary lattice  $\Lambda$ . One finds that when the gas  $B$  is in the MI regime, the time-averaged shifted Schmidt number reads

$$\langle\mathcal{K}_{AB}\rangle_t = 8L\alpha_A\alpha_Bz(2z-1)\lambda_A^2\lambda_B^2 \quad (\text{B.12})$$

for times satisfying (61). Moreover, Eq. (64) reads for an arbitrary lattice

$$\frac{1}{L}\mathcal{K}_{AB}(t) = 4\alpha_A\alpha_Bz\lambda_A^2\lambda_B^2\left[4z-2-4(z-1)\cos(tV)\cos(tU_B)-2\cos(2tV)\cos(tU_B)\right] \quad (\text{B.13})$$

if  $t \ll U_A^{-1}, J_B^{-1}, VU_B^{-2}$ .

## References

- [1] K. C. Wright, R. B. Blakestad, C. J. Lobb, W. D. Phillips, and G. K. Campbell, Phys. Rev. Lett. **110**, 025302 (2013).
- [2] C. Ryu, P. W. Blackburn, A. A. Blinova, and M. G. Boshier, Phys. Rev. Lett. **111**, 205301 (2013).
- [3] S. Eckel, J. G. Lee, F. Jendrzejewski, M. Murray, C. W. Clark, C. J. Lobb, W. D. Phillips, M. Edwards, and G. K. Campbell, Nature (London) **506**, 200 (2014).
- [4] B. T. Seaman, M. Krämer, D. Z. Anderson, and M. J. Holland, Phys. Rev. A **75**, 023615 (2007)
- [5] L. Amico and A. M. Boshier, in: *R. Dumke, Roadmap on Quantum Optical Systems*, Vol. **18** (Journal of Optics, 2016), p. 093001
- [6] D. S. Deaver and W. M. Fairbank, Phys. Rev. Lett. **7**, 43 (1961)
- [7] N. Byers and C. N. Yang, Phys. Rev. Lett. **7**, 46 (1961)
- [8] L. Onsager, Phys. Rev. Lett. **7**, 50 (1961)

- [9] L. P. Lévy, G. Dolan, J. Dunsmuir, and H. Bouchiat, *Phys. Rev. Lett.* **64**, 2074 (1990)
- [10] J. Dalibard, F. Gerbier, G. Juzeliunas, and P. Öhberg, *Rev. Mod. Phys.* **83**, 1523 (2011).
- [11] Y. Kagan, N. V. Prokofev, and B. V. Svistunov, *Phys. Rev. A* **61**, 045601 (2000)
- [12] T. Haug, J. Tan, M. Theng, R. Dumke, L-C. Kwek, and L. Amico, *Phys. Rev. A* **97**, 013633 (2018)
- [13] M. Cominotti, D. Rossini, M. Rizzi, F. Hekking, and A. Minguzzi, *Phys. Rev. Lett.* **113**, 025301 (2014)
- [14] D. Aghamalyan, M. Cominotti, M. Rizzi, D. Rossini, F. Hekking, A. Minguzzi, L. C. Kwek, R. Dumke, and L. Amico, *New. J. Phys.* **17**, 045023 (2015)
- [15] A. J. Leggett, *Prog. Theoret. Phys. Suppl.* **69**, 80 (1980)
- [16] D. W. Hallwood, T. Ernst, and J. Brand, *Phys. Rev. A* **82**, 063623 (2010)
- [17] D. Solenov and D. Mozyrsky, *Phys. Rev. A* **82**, 061601(R) (2010)
- [18] A. Nunnenkamp, A. M. Rey, and K. Burnett, *Phys. Rev. A* **84**, 053604 (2011)
- [19] C. Schenke, A. Minguzzi, and F. W. J. Hekking, *Phys. Rev. A* **84**, 053636 (2011)
- [20] P. Naldesi, J. P. Gomez, V. Dunjko, H. Perrin, M. Olshanii, L. Amico, and A. Minguzzi, *arXiv:1901.09398*
- [21] L. Kohn, P. Silvi, M. Gerster, M. Keck, R. Fazio, G. E. Santoro, and S. Montangero *Phys. Rev. A* **101**, 023617 (2020)
- [22] C. Kollath, A. M. Läuchli, and E. Altman, *Phys. Rev.* **98**, 180601 (2007)
- [23] G. Modugno, M. Modugno, F. Riboli, G. Roati, and M. Inguscio, *Phys. Rev. Lett.* **89**, 190404 (2002).
- [24] K. Günter, T. Stöferle, Henning Moritz, M. Köhl, and T. Esslinger, *Phys. Rev. Lett.* **96**, 180402 (2006).
- [25] S. B. Papp, J. M. Pino, and C. E. Wieman, *Phys. Rev. Lett.* **101**, 040402 (2008).
- [26] J. Catani, L. De Sarlo, G. Barontini, F. Minardi, and M. Inguscio, *Phys. Rev. A* **77**, 011603(R) (2008).
- [27] G. Thalhammer, G. Barontini, L. De Sarlo, J. Catani, F. Minardi, and M. Inguscio, *Phys. Rev. Lett.* **100**, 210402 (2008).
- [28] S. Sugawa, R. Yamazaki, S. Taie, Y. Takahashi, *Phys. Rev. A* **84**, 011610(R) (2011).
- [29] D. J. McCarron, H. W. Cho, D. L. Jenkin, M. P. Köppinger, and S. L. Cornish, *Phys. Rev. A* **84**, 011603(R) (2011).
- [30] I. Ferrier-Barbut, M. Delehaye, S. Laurent, A. T. Grier, M. Pierce, B. S. Rem, F. Chevy, and C. Salomon, *Science* **345**, 1035 (2014).
- [31] C. R. Cabrera, L. Tanzi, J. Sanz, B. Naylor, P. Thomas, P. Cheiney, and L. Tarruel, *Science* **359**, 301 (2017).

- [32] A. Kuklov and B. Svistunov, Phys. Rev. Lett. **90**, 100401 (2003).
- [33] A. Kuklov, N. Prokof'ev, and B. Svistunov, Phys. Rev. Lett. **92**, 030403 (2004).
- [34] A. Kuklov, N. Prokof'ev, and B. Svistunov, Phys. Rev. Lett. **92**, 050402 (2004).
- [35] C. Menotti and S. Stringari, Phys. Rev. A **81**, 045604 (2010).
- [36] Y. Li, M. R. Bakhtiari, L. He, and W. Hofstetter, Phys. Rev. B **84**, 144411 (2011).
- [37] Y. Li, L. He, and W. Hofstetter, New J. Phys. **15**, 093028 (2013).
- [38] L. Morales-Molina, S. A. Reyes, and E. Arevalo, EPL **115**, 36004 (2016).
- [39] V. Penna and A. Richaud, J. of Phys: Conf. Series **1206**, 012011 (2019).
- [40] I. Morera, G. E. Astrakharchik, A. Polls, and B. Juliá-Díaz, Phys. Rev. Research **2**, 022008(R) (2020).
- [41] K. Suthar, A. Roy, and D. Angom, Phys. Rev. A **91**, 043615 (2015)
- [42] K. Suthar and D. Angom, Phys. Rev. A **95**, 043602 (2017)
- [43] S. I. Mistakidis, G. C. Katsimiga, P. G. Kevrekidis, and P. Schmelcher, New J. Phys. **20**, 043052 (2018)
- [44] F. Meinert, M. Knap, E. Kirilov, K. Jag-Lauber, M. B. Zvonarev, E. Demler, and H.-C. Nägerl, Science **356**, 945 (2017)
- [45] F. Grusdt, G. E. Astrakharchik, and E. Demler, New J. Phys. **19**, 103035 (2017)
- [46] A. G. Volosniev and M.-W. Hammer, Phys. Rev. A **96**, 031601(R) (2017)
- [47] S. I. Mistakidis, G. C. Katsimiga, G. M. Koutenkakis, Th. Busch, and P. Schmelcher, Phys. Rev. Lett. **112**, 183001 (2019)
- [48] F. Theel, K. Keiler, S. I. Mistakidis, and P. Schmelcher, New J. Phys. **22**, 023027 (2020)
- [49] F. Meinert, M. J. Mark, E. Kirilov, K. Lauber, P. Weinmann, A. J. Daley, and H.-C. Nägerl, Phys. Rev. Lett. **111**, 053003 (2013).
- [50] F. Meinert, M. J. Mark, K. Lauber, A. J. Daley, and H.-C. Nägerl, Phys. Rev. Lett. **116**, 205301 (2016).
- [51] S. Greschner, G. Sun, D. Poletti, and L. Santos, Phys. Rev. Lett. **113**, 215303 (2014).
- [52] S. Campbell, M.A. García-March, T. Fogarty, and T. Busch, Phys. Rev. A **90**, 013617 (2014).
- [53] L. Morales-Molina, S. A. Reyes, and M. Orszag, Phys. Rev. A **86**, 033629 (2012).
- [54] P. Calbrese and J. Cardy, J. Stat. Phys. P04010 (2005)
- [55] A. M. Kaufman, M. E. Tai, A. Lukin, M. Rispoli, R. Schittko, P. M. Preiss, and M. Greiner, Science **353**, 794 (2016)
- [56] D. Spehner, J. Math. Phys. **55**, 075211 (2014).
- [57] R. Horodecki, P. Horodecki, M. Horodecki, and K. Horodecki, Rev. Mod. Phys. **81**, 865 (2009).

- [58] S.J. van Enk and C.W.J. Beenakker, Phys. Rev. Lett. **108**, 110503 (2012).
- [59] A. Elben, B. Vermersch, C.F. Roos, and P. Zoller, Phys. Rev. A **99**, 052323 (2019).
- [60] T. Brydges *et al.*, Science **364**, 260 (2019)
- [61] A. J. Daley, H. Pichler, J. Schachenmayer, and P. Zoller, Phys. Rev. Lett. **109**, 020505 (2012)
- [62] L. Corman, L. Chomaz, T. Bienaimé, R. Desbuquois, C. Weitenberg, S. Nascimbène, J. Dalibard, and J. Beugnon, Phys. Rev. Lett. **113**, 135302 (2014)
- [63] S. Eckel, F. Jendrzejewski, A. Kumar, C. J. Lobb, and G. K. Campbell, Phys. Rev.X **4**, 031052 (2014)
- [64] R. Mathew, A. Kumar, S. Eckel, F. Jendrzejewski, G. K. Campbell, M. Edwards, and E. Tiesinga, Phys. Rev. A **92**, 033602 (2015)
- [65] F. Gerbier, A. Widera, S. Fölling, O. Mandel, T. Gericke, and I. Bloch, Phys. Rev. Lett. **95**, 050404 (2005); *ibid*, Phys. Rev. A **72**, 053606 (2005).
- [66] L. Morales-Molina, S. A. Reyes, and E. Arevalo, EPL **131**, 36001 (2020)
- [67] K. Sengupta, N. Dupuis, Phys. Rev. A **71**, 033629 (2005)
- [68] L. Amico, D. Aghamalyan, F. Aukstol, H. Crepaz, R. Dumke, and L. C. Kwek, Sci. Rep. **4**, 4298 (2014)
- [69] R. Schmied and P. Treutlein, New J. Phys. **13**, 065019 (2011)
- [70] B. P. Lanyon *et al.*, Nature Physics **13**, 1158 (2017)
- [71] V. Penna and A. Richaud, Phys. Rev. A **96**, 053631 (2017)